Available online at www.sciencedirect.com

ScienceDirect

Geochimica et Cosmochimica Acta 187 (2016) 237–259

Geochimica et Cosmochimica Acta

www.elsevier.com/locate/gca

Elephant Moraine 96029, a very mildly aqueously altered and heated CM carbonaceous chondrite: Implications for the drivers of parent body processing

Martin R. Lee [a], Paula Lindgren [a,*], Ashley J. King [b], Richard C. Greenwood [c], Ian A. Franchi [c], Robert Sparkes [d]

[a] School of Geographical and Earth Sciences, University of Glasgow, Gregory Building, Lilybank Gardens, Glasgow G12 8QQ, UK
[b] Department of Earth Science, Natural History Museum (London), Cromwell Rd, London SW7 5BD, UK
[c] Planetary and Space Sciences, The Open University, Walton Hall, Milton Keynes MK7 6AA, UK
[d] Williamson Research Centre for Molecular Environmental Science, School of Earth, Atmospheric and Environmental Sciences, University of Manchester, Oxford Road, Manchester M13 9PL, UK

Received 19 August 2015; accepted in revised form 4 May 2016; available online 10 May 2016

Abstract

Elephant Moraine (EET) 96029 is a CM carbonaceous chondrite regolith breccia with evidence for unusually mild aqueous alteration, a later phase of heating and terrestrial weathering. The presence of phyllosilicates and carbonates within chondrules and the fine-grained matrix indicates that this meteorite was aqueously altered in its parent body. Features showing that water-mediated processing was arrested at a very early stage include a matrix with a low magnesium/iron ratio, chondrules whose mesostasis contains glass and/or quench crystallites, and a gehlenite-bearing calcium- and aluminium-rich inclusion. EET 96029 is also rich in Fe,Ni metal relative to other CM chondrites, and more was present prior to its partial replacement by goethite during Antarctic weathering. In combination, these properties indicate that EET 96029 is one of the least aqueously altered CMs yet described (CM2.7) and so provides new insights into the original composition of its parent body. Following aqueous alteration, and whilst still in the parent body regolith, the meteorite was heated to ~400–600 °C by impacts or solar radiation. Heating led to the amorphisation and dehydroxylation of serpentine, replacement of tochilinite by magnetite, loss of sulphur from the matrix, and modification to the structure of organic matter that includes organic nanoglobules. Significant differences between samples in oxygen isotope compositions, and water/hydroxyl contents, suggests that the meteorite contains lithologies that have undergone different intensities of heating. EET 96029 may be more representative of the true nature of parent body regoliths than many other CM meteorites, and as such can help interpret results from the forthcoming missions to study and return samples from C-complex asteroids.
© 2016 The Author(s). Published by Elsevier Ltd. This is an open access article under the CC BY license (http://creativecommons.org/licenses/by/4.0/).

Keywords: CM carbonaceous chondrites; Aqueous alteration; Thermal processing

1. INTRODUCTION

CM carbonaceous chondrites are samples of one or more primitive bodies, probably C-complex asteroids, and are valuable sources of information about the early history of the Solar System. These meteorites contain materials that have remained unchanged since being accreted from the protoplanetary disc (crystalline and amorphous silicates, oxides, metals, sulphides, organic matter) together with a suite of secondary minerals that formed by aqueous alteration of parent body interiors (principally phyllosilicates,

* Corresponding author.

http://dx.doi.org/10.1016/j.gca.2016.05.008
0016-7037/© 2016 The Author(s). Published by Elsevier Ltd.
This is an open access article under the CC BY license (http://creativecommons.org/licenses/by/4.0/).

carbonates, and Fe-rich oxides and sulphides) (e.g., McSween, 1979; Bunch and Chang, 1980). These secondary minerals are a major constituent of the fine-grained meteorite matrix, and also occur within chondrules, calcium- and aluminium-rich inclusions (CAIs), and their fine-grained rims. The CM meteorites show a range of degrees of aqueous alteration, which can be described using petrographic, mineralogical, chemical and isotopic properties (McSween, 1979; Browning et al., 1996; Rubin et al., 2007; Howard et al., 2009, 2011, 2015; Alexander et al., 2012, 2013).

The precursors to the secondary minerals are poorly understood because of the absence from our collections of unaltered CMs (i.e., that would be classified as CM3). By analogy with essentially unaltered members of other carbonaceous chondrite groups, namely the CR3 and CO3 meteorites and the ungrouped meteorite Acfer 094, the matrix and fine-grained rims of a hypothetical CM3 probably contained finely crystalline anhydrous silicates, metals and sulphides in an amorphous silicate groundmass (Brearley, 1993; Greshake, 1997; Abreu and Brearley, 2010). Chondrules and CAIs in a CM3 lithology would have contained only anhydrous minerals and glasses. Results from recent studies of several mildly altered CMs have allowed this analogy to be tested. These meteorites include Yamato (Y-) 791198 (Chizmadia and Brearley, 2008; Maeda et al., 2009), Queen Elizabeth Range (QUE) 97990 (Rubin et al., 2007; Maeda et al., 2009), and Paris (Hewins et al., 2014; Marrocchi et al., 2014; Rubin, 2014, 2015). Amorphous silicates occur in the matrices and fine-grained rims of Y-791198 and Paris, but almost all chondrules in the three meteorites contain phyllosilicates that formed by aqueous alteration of an original glass-dominated mesostasis (Richardson, 1981). Therefore even Y-791198, QUE 97990 and Paris do not preserve the full spectrum of the most reactive and ephemeral nebular components.

Some CMs were heated within their parent body and to temperatures that were sufficiently high to dehydroxylate, dehydrate and recrystallize alteration products, and recrystallize some of the primary minerals (e.g., Akai, 1990; Nakamura, 2005, 2006; Tonui et al., 2014). There are several possible drivers of this thermal processing (Akai, 1988). Meteorite parent bodies are widely believed to have been heated by the decay of short-lived radionuclides, principally ^{26}Al (e.g., Grimm and McSween, 1989). Sufficient heat was produced to melt accreted ices, and so generated the water that mediated aqueous alteration. If temperatures continued to rise, aqueous alteration would have passed into thermal metamorphism. Impacts have also been proposed as a source of the heat (e.g., Nakamura, 2005). Such a driver is consistent with evidence that the thermal processing was very brief (Nakato et al., 2008), and some of the heated meteorites have been deformed by shock (Nakamura, 2006). A third possibility is that a subset of the CMs experienced radiative heating as their parent body passed close to the Sun.

Here we present evidence that the degree of aqueous alteration of the Antarctic find Elephant Moraine (EET) 96029 is equal to, or even less than, the least altered CM carbonaceous chondrites that have been described to date. This meteorite can therefore bring us closer to understanding the nature of the progenitor of the CMs. Our work also, however, shows that EET 96029 was significantly heated after aqueous alteration, and it has evidence for Antarctic weathering. Thus, in order to understand the history of this meteorite, and so ascertain the original composition of its C-complex parent body, it is necessary to disentangle the competing and potentially self-reinforcing effects of mild aqueous processing, later heating, and terrestrial alteration. Owing to this unusual combination of properties, EET 96029 can also provide new insights into the environments and drivers of various agents of parent body processing.

2. MATERIALS AND METHODS

2.1. Meteorites studied

EET 96029 was recovered from Antarctica in 1996. It has a mass of 843.3 g, and a weathering grade of A/B (Grossman, 1998). The CM2 classification of this meteorite on petrologic grounds (Righter, 2010) is consistent with its reflectance spectra (Cloutis et al., 2012). According to Grossman (1998) EET 96029 is paired with 10 other Antarctic finds: EET 96005, 06, 07, 11, 12, 13, 14, 16, 17, 19. The present study used three samples of EET 96029, comprising one thin section and two rock chips. The rock chips were sub-sampled for various analyses, and an additional thin section was made from one of them. The sizes of these samples and the techniques that were used to study them are listed in Table 1. Six other CM carbonaceous chondrites were also analysed in order to provide comparative data to aid in the interpretation of results from Raman spectroscopy and thermogravimetric analysis (Table 1).

2.2. Scanning electron microscopy (SEM) and X-ray microanalysis

SEM work was undertaken in the Imaging Spectroscopy and Analysis Centre (ISAAC), University of Glasgow. Backscattered electron (BSE) imaging and energy-dispersive X-ray analysis (EDX) of thin sections used two SEMs, a FEI Quanta and a Zeiss Sigma, both operated at 20 kV. The Quanta is equipped with an EDAX Genesis microanalysis system and the Zeiss with an Oxford Instruments AZTEC system; both acquire X-rays through silicon-drift detectors. The sizes of chondrules and CAIs were determined from BSE images. For each object two measurements were taken, the long axis and the longest dimension normal to the long axis. The size of the object is expressed as the mean of these two measurements. Point counting used the Quanta SEM whereby the stage was moved in a grid pattern and the material in the centre of the field of view was identified at each point. EDX maps with a resolution of ~300 nm/pixel were acquired over a period of over ~30 min using the Zeiss SEM operated at 3 nA. The protocol for quantitative analysis is described in Appendix A.

2.3. Transmission electron microscopy (TEM)

TEM work and allied sample preparation was undertaken in the Kelvin Nanocharacterisation Centre (KNC),

Table 1
Meteorite samples used in the present study.

Meteorite	Thin section size (mm^2)/rock chip or powder mass (mg)	Techniques used for sample analysis
Cold Bokkeveld BM1727[a]	~2 mg	Raman spectroscopy of organic matter
EET 96029,9[b]	145 mm^2	SEM imaging, point counting, X-ray microanalysis, Raman spectroscopy, TEM
EET 96029,56-a[b]	42 mm^2	SEM imaging, X-ray microanalysis
EET 96029,56-b[b]	~2 mg	Raman spectroscopy of organic matter
EET 96029,56-c[b]	~5 mg (two replicates)	Bulk oxygen isotope analysis
EET 96029,57,21 (AK-1)[b]	8.54 mg	PSD-XRD, TGA
EET 96029,57,21 (AK-2)[b]	50 mg	PSD-XRD
	12.79 mg	TGA
	10.2 mg (two replicates)	Bulk oxygen isotope analysis
LON 94101,67 (a)[b]	~2 mg	Raman spectroscopy of organic matter
LON 94101,67 (b)[b]	~2 mg	Raman spectroscopy of organic matter
Murchison BM1988, M23[a]	~2 mg	Raman spectroscopy of organic matter
Murchison[c]	10–15 mg	TGA
PCA 91008,25[b]	~2 mg	Raman spectroscopy of organic matter
QUE 93005,31[b]	~2 mg	Raman spectroscopy of organic matter
SCO 06043,27[b]	~2 mg	Raman spectroscopy of organic matter

PSD-XRD denotes position sensitive detector X-ray diffraction.
TGA denotes thermogravimetric analysis.
[a] Loaned by the NHM.
[b] Loaned by NASA ANSMET.
[c] Five samples of Murchison from the NHM. Museum numbers unknown.

University of Glasgow. Electron-transparent foils were manufactured using a FEI Duomill® dual-beam focused ion beam (FIB) instrument that is equipped with a field-emission electron gun and a Ga^+ ion gun. Following the procedure of Lee et al. (2003), foils were cut from the EET 96029,9 thin section using 30 kV Ga^+ ions at a range of beam currents. The foils were initially milled to a thickness of ~1 μm, then extracted using an in-situ micromanipulator, welded to the tines of a copper holder using electron- and ion-deposited platinum, and finally milled to a thickness of ~100 nm. Bright-field images and selected area electron diffraction (SAED) patterns were obtained using a FEI T20 TEM operated at 200 kV. The foils were further ion milled to ~60 nm for subsequent scanning TEM (STEM) imaging, EDX analysis and electron energy loss spectroscopy work using a JEOL ARM200cF aberration-corrected instrument that was operated at 200 kV.

2.4. Raman spectroscopy

Raman spectroscopy was undertaken at ISAAC. This technique was used to identify minerals in thin section and to determine the structure of carbon in powdered bulk samples. Carbon is useful for reconstructing CM thermal history since it typically increases in structural order with heating (Quirico et al., 2014). To provide an internal comparison, six CMs were analysed along with EET 96029, some of which have been heated naturally (Tables 1 and 2). Raman spectra were acquired using a Renishaw inVia microscope that is equipped with a 514 nm laser. Focusing of the laser was performed through a petrographic microscope with a 100× objective. The spectra were accumulated in 12 increments, each measured over two seconds and using 100% of the total laser power of 50 mW. The spot size was typically 1 μm. Calibration was undertaken with respect to wavenumber using a Si standard. Appendix A provides further details of data processing and interpretation.

2.5. Position sensitive detector X-ray diffraction (PSD-XRD)

X-ray diffraction (XRD) work was undertaken at the Natural History Museum, London (NHM). For the initial identification of phases within a powdered fragment (8.54 mg) of EET 96029,57,21 (AK-1), an XRD pattern was collected using an INEL X-ray diffractometer with a curved 120° position sensitive detector (PSD) in a static geometry relative to the X-ray beam and sample. The sample was mounted on a low background single crystal sapphire substrate and analysed using Co $K\alpha_1$ radiation for 22 h. Silicon and silver behenate were used for calibration, and phases in the meteorite were identified using the International Centre for Diffraction Data (ICDD) database (PDF-2). Modal mineral abundances were obtained from a larger (~50 mg) chip of EET 96029,57,21 (AK-2) that was free of fusion crust. The chip was ground to <35 μm in order to minimise potential grain size artifacts, then loaded into an aluminium sample well using the sharp edge of a spatula. This packing method creates a high degree of randomness in grain orientation and reduces the effects of preferred crystal alignments (Batchelder and Cressey, 1998). For these measurements a second PSD-XRD was used with Cu $K\alpha_1$ radiation. The X-ray beam was at an incident angle of 4.2° to the flat top of the rotating sample, and the size of the beam was restricted to 0.24 × 2.00 mm

Table 2
Metrics of aqueous alteration and evidence for heating for the CMs studied or discussed.

CM meteorite	Petrologic subtype[a]	Phyllosilicate fraction[b]	H in water/OH[c]	Evidence for heating[c]
ALHA 81002	–	1.4	1.3	No
Cold Bokkeveld	CM2.2	1.4	1.3	No
EET 96029	CM2.7[d]	1.6[d]	2.0[f]	Yes[d]
LON 94101	–	1.4	1.8	No
MET 01070	CM2.0	1.2	1.2	No
MET 01072	–	–	1.5	Yes
Mighei	–	1.4	1.6	No
Murchison	CM2.5	1.5	1.6	No
Murray	CM2.4/2.5	1.5	1.5	No
Niger (I)	–	–	–	–
Paris	CM2.7[e]	–	–	No[g]
PCA 91008	–	–	–	Yes[f]
QUE 93005	CM2.1	1.3	1.4/1.5	Yes
QUE 97990	CM2.6	1.6	1.7	No
SCO 06043	–	1.2	1.1/1.2	No
Y-75293	–	–	–	–
Y-790123	–	–	–	–
Y-791198	CM2.4	1.6	1.5	No
Y-793321	–	–	–	Yes[h]

– Denotes unknown.
[a] After Rubin et al. (2007) unless otherwise stated.
[b] Howard et al. (2015).
[c] After Alexander et al. (2013) unless otherwise stated.
[d] From the present study.
[e] From Marrocchi et al. (2014) and Rubin (2015).
[f] Calculated from data in Alexander et al. (2012).
[g] Hewins et al. (2014).
[h] Nakamura (2006).

using post monochromator slits. The XRD pattern for EET 96029,57,21 (AK-2) was collected for 16 h; patterns of mineral standards were acquired under the same experimental conditions for 30 min. Differences in the incident beam flux throughout the experimental run were monitored by analysing a polished block of Fe metal at the start of each day. Details of phase quantification are in Appendix A.

2.6. Thermogravimetric analysis (TGA)

The TGA work was undertaken at the NHM using a TA instruments SDT Q600. The whole of EET 96029,57,21 (AK-1, 8.54 mg) and a 12.79 mg aliquot of EET 96029,57,21 (AK-2) were analysed. Each sample was powdered, and then stored in a glass vial within a desiccator. These samples were loaded into an alumina crucible and analysed under a N_2 flow of 100 ml min^{-1}. The mass of the sample was recorded as it was heated from 25 to 1000 °C at a rate of 10 °C min^{-1}. The balance sensitivity of the TGA is 0.1 μg and the overall error on the measured mass loss fraction is ~0.1%. DTG curves (wt.% per °C) show the change in mass loss with heating. Peak positions as a function of temperature are characteristic of mineral groups and individual phases. Weakly bonded H_2O (probably terrestrial contamination) is liberated up to 200 °C, dehydration and dehydroxylation of Fe-(oxy) hydroxides occurs from 200 to 400 °C, and dehydroxylation of phyllosilicates from 400 to 770 °C. Carbonates decompose at 770–900 °C (Garenne et al., 2014; King et al., 2015a).

2.7. Oxygen isotope analysis

The oxygen isotopic compositions of bulk samples of EET 96029,56-c and EET 96029,57,21 (AK-2) were determined at the Open University (OU) using a modified version of the infrared laser fluorination system described by Miller et al. (1999). Details of the technique are in Appendix A. Published analytical precision (2σ) for the OU system, based on replicate analyses of international (NBS-28 quartz, UWG-2 garnet) and internal standards, is approximately ±0.08‰ for $\delta^{17}O$; ±0.16‰ for $\delta^{18}O$; ±0.05‰ for $\Delta^{17}O$ (Miller et al., 1999). Changes to analytical procedures implemented after the system description in Miller et al. (1999) have yielded improvements to precision such that 39 analyses of an internal obsidian standard undertaken during six separate sessions in 2013 gave the following combined results: ±0.05‰ for $\delta^{17}O$; ±0.09‰ for $\delta^{18}O$; ±0.02‰ for $\Delta^{17}O$ (2σ). Oxygen isotope results are reported in standard δ notation, where $\delta^{18}O$ has been calculated as: $\delta^{18}O = [(^{18}O/^{16}O)_{sample}/(^{18}O/^{16}O)_{ref} - 1] \times 1000$ (‰) and similarly for $\delta^{17}O$ using the $^{17}O/^{16}O$ ratio, the reference being Vienna Standard Mean Ocean Water (VSMOW). For the purposes of comparison with the results of previous authors $\Delta^{17}O$, which represents the deviation from the terrestrial fractionation line, has been calculated as: $\Delta^{17}O = \delta^{17}O - 0.52 \times \delta^{18}O$.

3. RESULTS

3.1. Properties of the bulk meteorite

3.1.1. Mineralogy

PSD-XRD results show that EET 96029,57,21 (AK-1 and AK-2) contains the following minerals (in vol.%): enstatite (15.7), olivine (12.2), magnetite (3.1), Fe-sulphide (2.4), calcite (1.0), gypsum (1.0), Fe,Ni metal (0.3) (Fig. 1). After subtracting the crystalline phases from the pattern during profile-stripping, the residual did not reduce to zero and the sum of the fit factors was less than one. This result indicates that EET 96029,57,21 has a non-crystalline constituent. The shape and intensity of the residual was in good agreement with the diffuse features of the phyllosilicate standard, so the remaining 64.7 vol.% is attributed to degraded phyllosilicates, which are characteristic of heated CM and CI chondrites (Nakamura, 2005; King et al., 2015b). The presence of amorphous nebular silicates and finely crystalline Fe-(oxy)hydroxides cannot be ruled out, although as the residual could be reduced to zero, their abundance must be low.

3.1.2. Abundance of water/OH

TGA was undertaken on two sub-samples of EET 96029,57,21 (AK-1 and AK-2). Over the 25–900 °C range they lost 23.1% and 19.5% of their original weight (Table 3). Approximately equal amounts of water were released in the 25–200 °C (the range ascribed to removal of terrestrial water) and 400–770 °C steps (the range ascribed to phyllosilicate breakdown). In Table 3 these data are compared with TGA results from EET 96029 in Garenne et al. (2014), who recorded a significantly lower weight loss of 14.0% over the 25–900 °C temperature range.

3.1.3. Oxygen isotope composition

Two replicate analyses of EET 96029,56-c and EET 96029,57,21 (AK-2) were obtained (Table 4). In an oxygen three-isotope plot these analyses lie at almost opposite ends of the range of CM compositions (Fig. 2). EET 96029 was also analysed by Tyra et al. (2007), and their data plot close to EET 96029,57,21 (AK-2) at the isotopically light end of the CM field (Fig. 2).

3.2. Petrography and mineralogy of EET 96029

EET 96029,9 and EET 96029,56-a both lack a compactional petrofabric, and veins of terrestrial sulphates and carbonates are absent (Lindgren et al., 2015) (Fig. 3). SEM point counting shows that the principal constituents of EET 96029,9 are the matrix (77.76 vol.%), chondrules (16.74 vol.%), fine-grained rims (3.70 vol.%) and CAIs (1.80 vol.%) (Table 5). No clasts were identified in these two samples.

3.2.1. Properties of the matrix and fine-grained rims

Quantitative analysis of cation oxides in the fine-grained matrix gives a mean total of 83.55 ± 3.32 wt.% (Table 6; Fig. 4). These results indicate the presence of minerals containing water/OH, although other factors may contribute to lowering the totals (e.g., the presence of micropores, and the lower density of amorphous materials relative to the analytical standards). The elemental composition of this fine-grained material lies close to serpentine (Fig. 5), and is consistent with the identification of Fe^{2+}-bearing serpentine in reflectance spectra of EET 96029 (Cloutis et al., 2012). As regards the MgO/FeO ratio, which in CM matrices varies with the degree of alteration, EET 96029,9 has a value of 0.35, as compared with 0.39 for Paris (Table 6). Another diagnostic ratio is S/SiO_2, which is significantly lower in EET 96029,9 than Paris (0.08 versus 0.15, respectively; Table 6). TEM shows that fine grained rims contain patches of a compact material that are a few micrometres in size. These patches are composed of nanoscale fibres within an amorphous groundmass (Fig. 6a and b). The fine grained rim material between

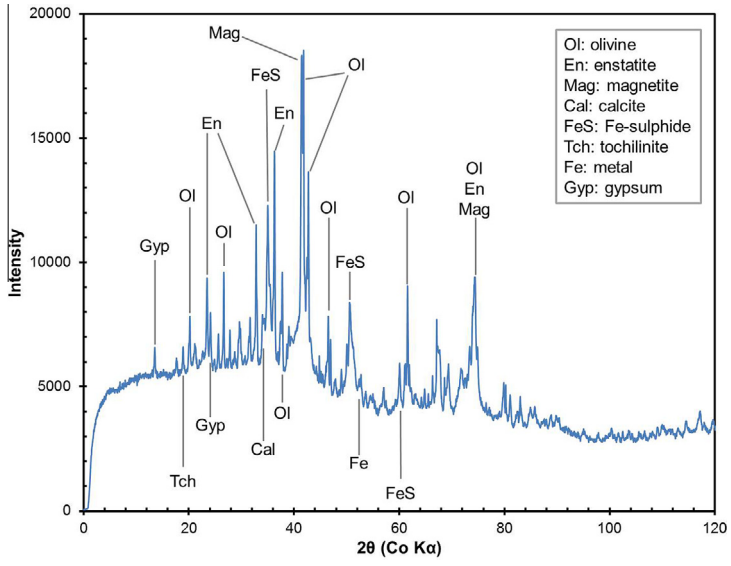

Fig. 1. PSD-XRD pattern of EET 96029,57,21 (AK-1) with the main peaks labelled.

Table 3
Thermogravimetric analysis results from EET 96029 compared with data from Murchison.

Temperature step (°C)	Mass loss (wt.%)				
	EET 96029,57,21			Murchison	
	AK-1	AK-2	Garenne et al. (2014)	NHM	Garenne et al. (2014)
25–200	9.2	8.0	5.1	4.3 (0.3)	2.7
200–400	2.1	2.5	3.7	4.0 (0.2)	3.5
400–770	9.4	7.9	4.5	6.9 (0.2)	7.3
770–900	2.4	1.1	0.7	1.1 (0.0)	1.9
Total	23.1	19.5	14.0	16.3 (0.7)	15.4

AK-1 and AK-2 have masses of 8.54 and 12.79 mg, respectively.
NHM denotes the mean of five samples of Murchison analysed for the present study.
Values in parentheses are the 1σ standard deviations.

Table 4
Oxygen isotope compositions of bulk samples of EET 96029.

	$\delta^{17}O$ (‰)	1σ	$\delta^{18}O$ (‰)	1σ	$\Delta^{17}O$ (‰)	1σ
EET 96029,56-c						
Replicate 1	3.22		10.71		−2.35	
Replicate 2	3.36		10.94		−2.33	
Mean	3.29	0.10	10.82	0.17	−2.34	0.02
EET 96029,57,21 (AK-2)						
Replicate 1	−1.42		3.52		−3.25	
Replicate 2	−1.00		4.14		−3.15	
Mean	−1.21	0.30	3.83	0.44	−3.20	0.07
EET 96029[a]	−2.6	0.1	2.4	0.2	−3.82	0.05

[a] From Tyra et al. (2007).

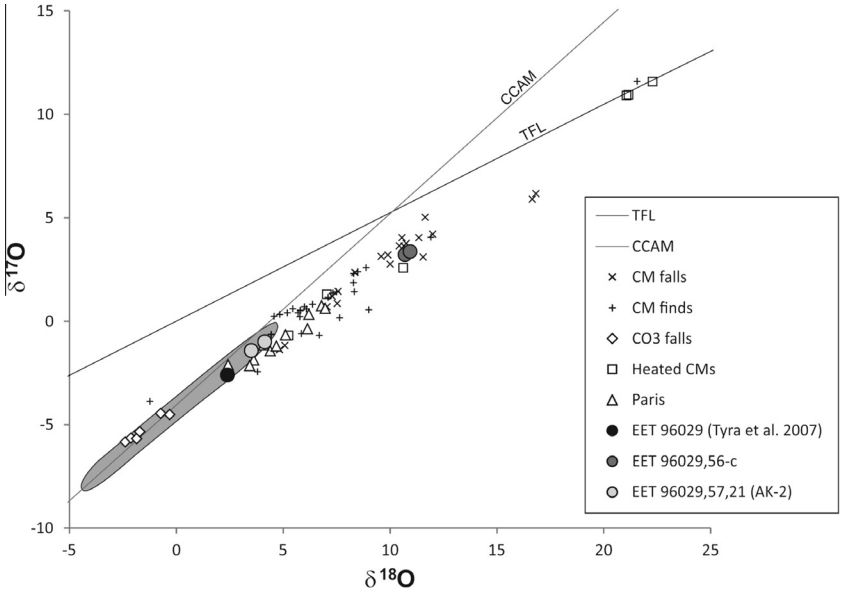

Fig. 2. Oxygen three isotope plot showing analyses of EET 96029-c (this study), EET 96029,57,21 (AK-2) (this study) and EET 96029 (Tyra et al., 2007). Data from other carbonaceous chondrites are shown for comparison. The CM falls are from Clayton and Mayeda (1999), Grossman and Zipfel (2001), Haack et al. (2012) and Jenniskens et al. (2012). CM finds are from Clayton and Mayeda (1999), Tyra et al. (2007), Moriarty et al. (2009) and Pernet-Fisher et al. (2014). CO3 falls are from Clayton and Mayeda (1999). Heated CMs are from Tonui et al. (2003, 2014), and Paris data are from Hewins et al. (2014). The oval shaded area is the CV envelope was constructed using data in Clayton and Mayeda (1999). TFL denotes the terrestrial fractionation line and CCAM the carbonaceous chondrite anhydrous mineral line.

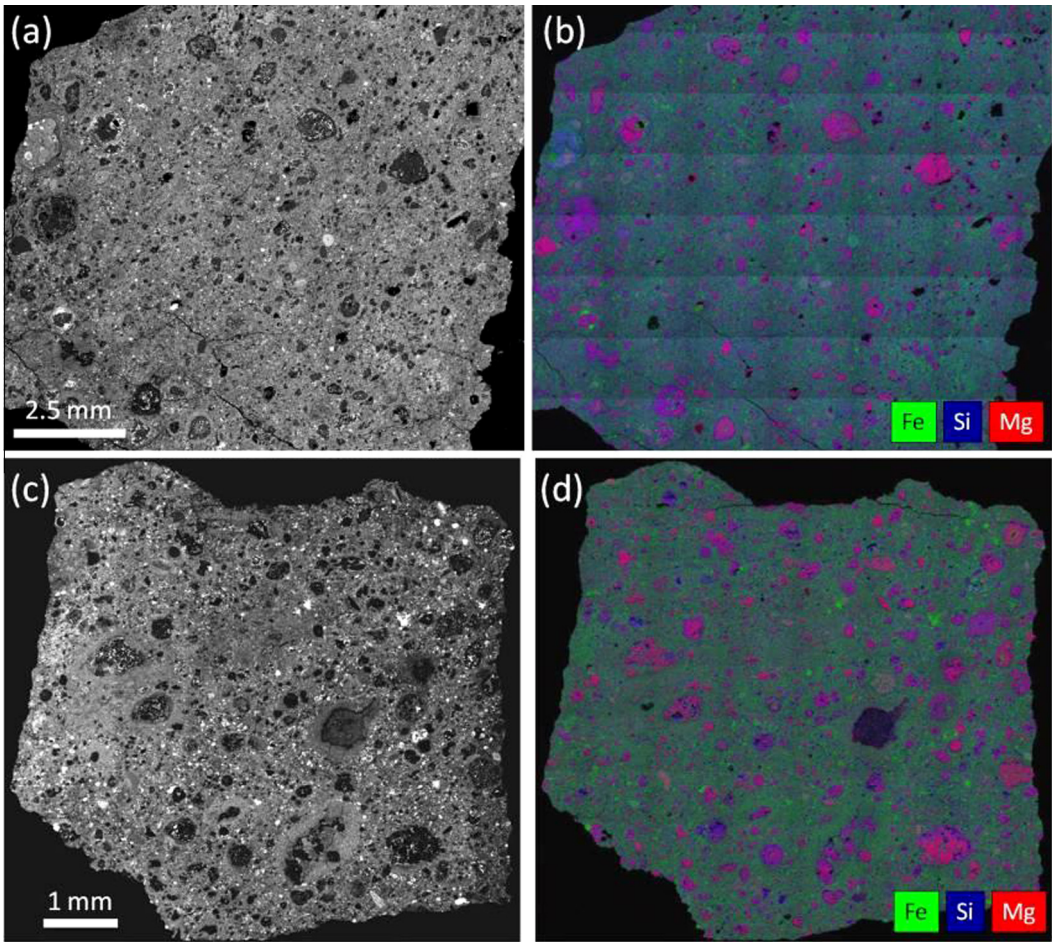

Fig. 3. (a) BSE image of EET 96029,9. (b) Corresponding false coloured X-ray map made by blending maps for Mg (red), Si (blue) and Fe (green). (c) BSE image of EET 96029,56-a. (b) Corresponding false coloured X-ray map made by blending maps for Mg (red), Si (blue) and Fe (green). In the two X-ray maps the matrix is turquoise whereas Mg-rich olivine and pyroxene grains are purple. (For interpretation of the references to colour in this figure legend, the reader is referred to the web version of this article.)

Table 5
The abundance of constituents of EET 96029,9 matrix and chondrules as determined by point counting.

Matrix constituents	Vol.%	Chondrule constituents	Vol.%
Fine-grained material	63.43	Silicate mineral grains	13.17
Silicate mineral grains	6.17	Mesostasis phyllosilicate	1.50
Fe–S–O clumps	5.03	Fe-(oxy)hydroxide after Fe,Ni metal	0.60
Sulphides	1.07	Phyllosilicate within silicate mineral grains	0.57
Calcite	0.93	Mesostasis quench crystallites	0.37
Fe-(oxy)hydroxide after Fe,Ni metal	0.80	Fe,Ni metal	0.23
Sulphide alteration products	0.13	Sulphides	0.07
Xenolithic clasts	0.10	Sulphide alteration products	0.23
Fe,Ni metal	0.10		
Total	77.76	Total	16.74

EET 96029,9 has a modal mineralogy of 77.76 vol% matrix, 16.74 vol.% chondrules, 3.70% fine-grained rims, 1.80 vol.% CAIs.
$n = 3000$ points, excluding porosity.
Point counting used a SEM at a magnification of ×2000 and a step size of 150 μm.

patches contains a high density of sub-micrometre sized pores, at the edges of some of which are organic nanoglobules (Fig. 6a and c).

The only carbonate mineral indentified is calcite, which occurs mainly as scarce grains in the matrix (Lee et al., 2014). Tyra et al. (2007) also found small quantities of

Table 6
Chemical composition (wt.%) of the matrices of EET 96029 and Paris.

	EET 96029,9	Paris
SiO_2	28.0 (3.1)	27.1 ± 1.5
Al_2O_3	3.1 (0.5)	2.5 ± 0.3
FeO	34.3 (6.2)	34.0 ± 2.0
NiO	2.12 (0.75)	–
Cr_2O_3	0.38 (0.17)	0.28 ± 0.05
MnO	0.15 (0.15)	0.21 ± 0.04
MgO	12.1 (2.1)	13.2 ± 1.2
CaO	0.31 (0.24)	0.34 ± 0.21
Na_2O	0.59 (0.16)	1.0 ± 0.2
K_2O	0.06 (0.08)	0.08 ± 0.02
S	2.2 (1.0)	4.2 ± 0.8
P_2O_5	0.28 (0.07)	–
Total	83.55 (3.32)	82.91
n	28	10
MgO/FeO	0.35 (0.13)	0.39
S/SiO_2	0.08 (0.04)	0.15

Paris data from Rubin (2015).
– denotes not analysed for.
n denotes number of analyses.
Figures in parentheses are 1σ standard deviations.
The method for determining errors of the Paris data was not stated.

calcite in EET 96029. Organic carbon was identified by Raman spectroscopy, and results from EET 96029,56-b along with data from six CMs are plotted in Fig. 7. PCA 91008 has been naturally heated, and has a higher D/G (intensity) and a lower D (FWHM) than the other CMs. EET 96029,56-b has a slightly higher D/G (intensity) than five of the analysed meteorites.

3.2.2. Fe,Ni metal and sulphides in the matrix and chondrules

Fe,Ni metal comprises 0.33 vol.% of EET 96029,9 (Table 5). It is more abundant in chondrules than the matrix, and grains range in size from ~1 to 200 μm. All of the grains that were qualitatively chemically analysed are Ni-poor (kamacite) and internally homogeneous. More Fe,Ni metal was formerly present in the chondrules but has been altered to Fe-(oxy)hydroxides, which comprise 1.40 vol.% of EET 96029,9 (Table 5). The chondrule in Fig. 8a provides an example of such alteration. It contains two grains with cores of Fe,Ni metal and concentrically layered rims that are rich in O and Fe and contain goethite, as identified by Raman spectroscopy (Fig. 8a–c). EET 96029,9 has 1.14 vol.% Fe-rich sulphide, most of which occurs in the matrix as grains ~16–84 μm in size (Table 5). The majority of these grains are composed of pyrrhotite with micrometre-sized lamellae or blebs of pentlandite (Fig. 8d and e). Individual grains of pentlandite are absent, although two sulphide grains have average atomic Ni/(Ni + Fe) values of 0.39 and 0.41, which lie at the boundary between intermediate sulphide and pentlandite (Fig. 9).

The matrix contains rounded objects that are typically a few tens of micrometres in diameter, often contain calcite grains, and are rich in Fe, S and O (Lee et al., 2014) (Fig. 10). These 'Fe–S–O clumps' constitute 5 vol.% of EET 96029,9. Raster analyses yield element ratios that are similar to those of 'type II PCP' (serpentine intergrown with tochilinite; Tomeoka and Buseck, 1985) (Fig. 11). The clumps comprise laths that lie in a lower Z groundmass. Individual laths contain O, S, Fe and Ni (Fig. 11), and their SAED patterns index as magnetite (Fig. 10b and c); no sulphide minerals were identified by TEM. The groundmass is rich in O, Mg, Si and Fe, and yields SAED patterns with indistinct reflections that indicate a poor crystallinity.

3.2.3. Chondrule mineralogy

EET 96029,9 chondrules have a mean size of 400 ± 220 μm (1σ; $n = 18$). Of the 18 chondrules that were studied in detail, 12 are type I and six are type II. Olivine phenocrysts in the type I and II chondrules have mean compositions of $Fo_{98\pm2\%}$ (1σ, $n = 57$ grains) and $Fo_{67\pm6\%}$ (1σ, $n = 67$ grains), respectively. Phyllosilicates are present in the mesostasis of all type I chondrules and in all but one of the type II chondrules. The phyllosilicate-free chondrule (EETC-4) has a glass mesostasis and is described first.

3.2.3.1. Chondrule EETC-4. EETC-4 is a type IIA chondrule (Fig. 12a and b). It contains euhedral crystals of olivine ($Fo_{\sim69}$), between which is a mesostasis that has a dominant Si-rich component and a subordinate Fe-rich component. The Si-rich mesostasis principally contains O, Al, Si and Fe (Table 7; Fig. 5), and its analytical totals of 97 wt.% may reflect the presence of water. The main constituent of the Si-rich mesostasis is a glass with quench crystallites, grains of Fe,Ni metal and spherules of Fe-sulphide (Fig. 12c and d). EDX maps show that the glass is rich in O, Na, Al and Si, whereas the quench crystallites contain O, Mg, Si, Ca and Fe. The crystallites were too small to individually analyse by EDX, but assuming that the glass has an Al/Si ratio (by weight) of 2.25, the quench crystallites have a composition of $Mg_{0.3}Ca_{1.0}Fe_{0.7}Si_2O_6$ (i.e., hedenbergite). This mineralogy was confirmed by indexing their SAED patterns. Fe-sulphide spherules range in diameter from ~50 to 200 nm. One of the largest, which is 200 nm in diameter, contains O and Fe, but is free of S.

The Fe-rich mesostasis forms patches up to ~10 μm in size that may enclose quench crystallites (Fig. 12a and e). Relative to Si-rich mesostasis it is depleted in Na, Al, Si, and Ca, and enriched in Mg, S, Fe and Ni (Fig. 5, Table 7). SAED patterns of the Fe-rich mesostasis contain rings with *d*-spacings of 0.252, 0.205, 0.170, 0.160 and 0.145 nm, which are consistent with 6-line ferrihydrite (Janney et al., 2000). The compositional range of these patches therefore reflects the presence within the analysed volume of ferrihydrite, glass, and quench crystallites.

3.2.3.2. Phyllosilicate-bearing chondrules. In a (Si + Al)–Mg–Fe ternary diagram the phyllosilicate mesostasis of types I and II chondrules plot close to the meteorite's fine-grained matrix, thus suggesting that serpentine is abundant (Fig. 5). Mean analytical totals of 87.81 wt.% are consistent with the presence of water/OH (Fig. 4). The mesostasis contains grains with a layered microstructure that are ~2–3 μm in size and lie in a finer grained groundmass (Fig. 13a). SAED patterns show that these grains are poorly crystalline and so their mineralogy could not be determined (Fig. 13a). Out of the 18 chondrules that were

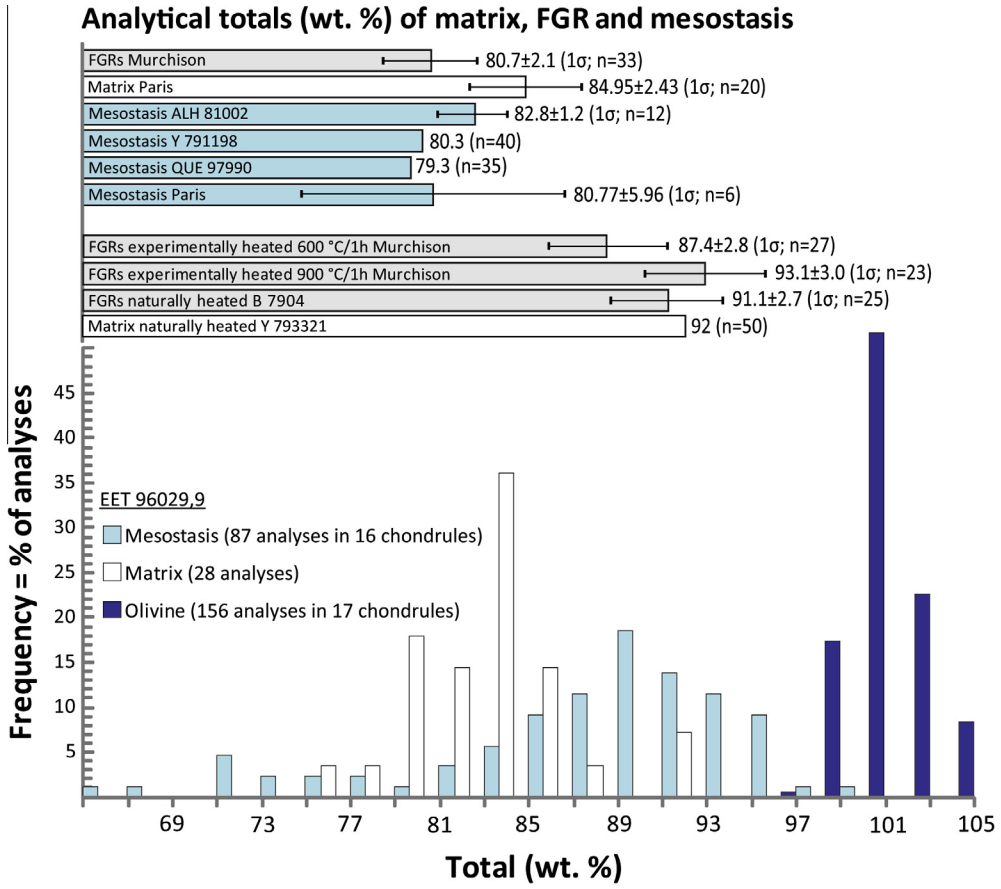

Fig. 4. Analytical totals obtained by X-ray microanalysis of various components of CM carbonaceous chondrites. The upper chart shows the mean totals obtained from fine grained rims (FGRs) of Murchison (unheated and experimentally heated to two temperatures) and the naturally heated Antarctic find B 7904 (Nakato et al., 2008). Also plotted are the matrices of Paris (Hewins et al., 2014) and Y-793321 (Nakamura, 2006), and phyllosilicate mesostases of ALH 81002 (Hanowski and Brearley, 2001), Y791198 and QUE 97990 (Maeda et al., 2009), and Paris (Hewins et al., 2014). The lower chart shows the totals obtained from EET 96029,9 fine-grained matrix (average 83.55 ± 3.32 (1σ; $n = 28$)) and altered chondrule mesostasis (average 87.81 ± 7.18 (1σ; $n = 87$ analyses in 16 chondrules)). For reference the analytical totals obtained from chondrule olivine grains are also plotted.

studied in detail, nine contain quench crystallites (Fig. 13b and c) or pores of a similar size and shape (i.e., moulds of crystallites; Fig. 13d). These crystallites are equally as abundant in type I and type II chondrules. Narrow phyllosilicate veins cross-cut olivine phenocrysts in a small proportion of the type I chondrules. Olivine grains in two of the EET 96029,9 type II chondrules have etched margins, and their interiors contain veins of fine-grained alteration products with serrated walls. Grains of clinopyroxene in type I and II chondrules commonly contain abundant micropores and narrow cracks. These intracrystalline structures are most likely to have formed during the transformation of protoenstatite to clinoenstatite (Hanowski and Brearley, 2001).

3.2.4. Abundance and mineralogy of CAIs

CAIs comprise 1.8 vol.% of EET 96029,9. The 23 that were studied in detail range in size from ~40 to ~200 μm (mean 100 ± 48 μm, 1σ; value excludes the fine-grained rim). Three morphological types of CAIs (Rubin, 2007) can be recognised: banded (61%), nodular (35%), and simple (4%). Of these 48% are intact. All of them contain aluminous spinel, 70% have pyroxene, 43% perovskite, 26% hibonite, 4% corundum and 4% contain gehlenite (Fig. 14a and b). Chemical analysis of the gehlenite yielded a mineral formula of $Ca_{2.02}Al_{0.74}Fe_{0.02}Mg_{0.13}(Al_{1.00}Si_{1.11})O_7$, and its presence is of note given the scarcity of this mineral in CAIs from other CMs (Greenwood et al., 1994; Rubin, 2007). Fe-rich phyllosilicates occur in 52% of the CAIs, and occur most commonly as a layer within banded inclusions. In one of these CAIs the phyllosilicate has a hexagonal pattern of fractures that is reminiscent of desiccation cracks in terrestrial sediments (Fig. 14c). The CAI-hosted phyllosilicates have been previously interpreted to have formed by aqueous alteration of melilite (e.g., gehlenite) (Greenwood et al., 1994; Lee and Greenwood, 1994).

4. DISCUSSION

The mineralogy and composition of EET 96029 are consistent with it having undergone unusually mild aqueous alteration. This meteorite therefore has the potential to

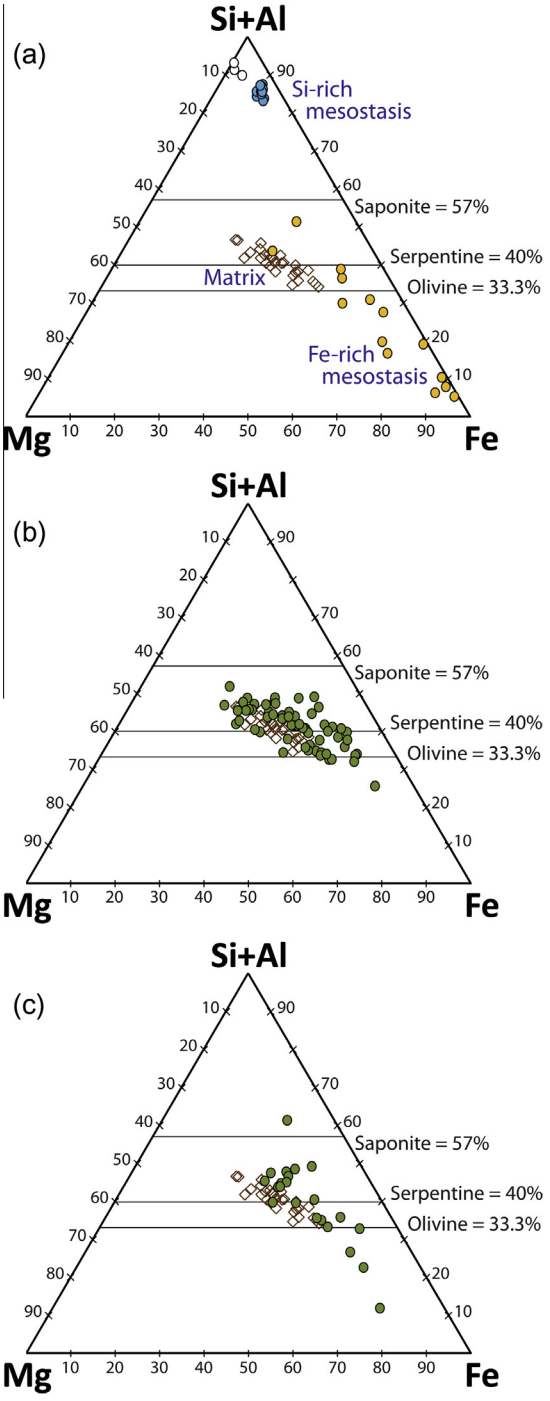

Fig. 5. Ternary diagrams (at.%) showing the compositions of various components of EET 96029,9. All three diagrams include the matrix (open diamonds) and element ratios for stoichiometric olivine, saponite and serpentine. (a) Si-rich mesostasis (blue circles) and Fe-rich mesostasis (orange circles) in chondrule EETC-4. Also plotted is glass in chondrules from other CMs (white circles; data in Table 5). (b) Phyllosilicate mesostasis of type I chondrules ($n = 65$ analyses from 11 chondrules). (c) Phyllosilicate mesostasis of type II chondrules ($n = 22$ analyses from 4 chondrules). (For interpretation of the references to colour in this figure legend, the reader is referred to the web version of this article.)

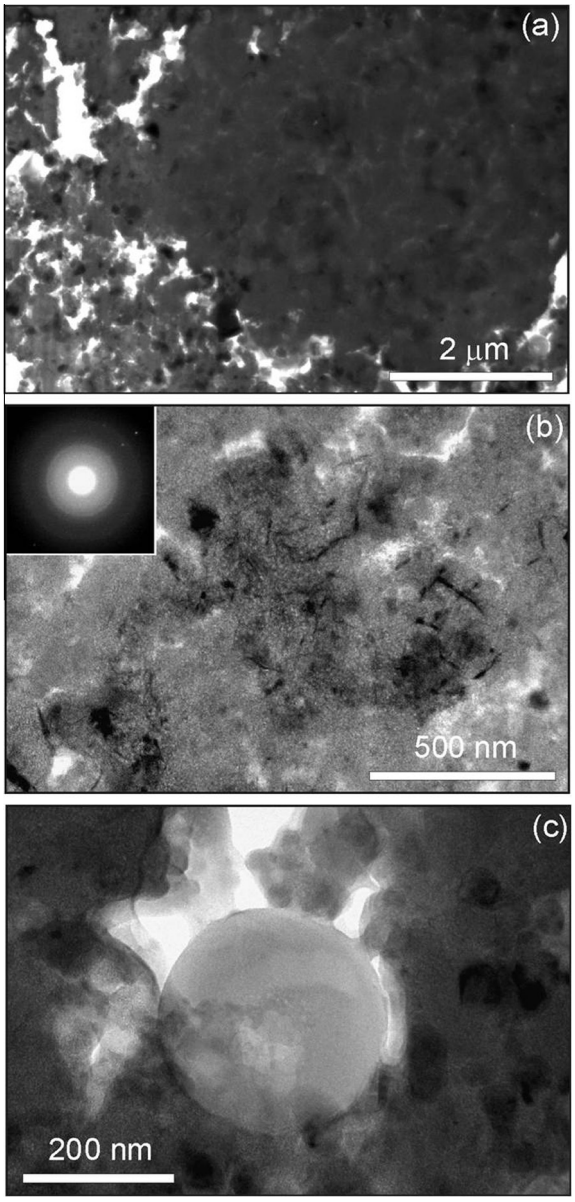

Fig. 6. Bright-field TEM images of a fine-grained rim in EET 96029,9. Holes in the foil, which correspond approximately to original pore spaces, are white. (a) An area of the rim containing a patch of compact material (right hand side) and micropore-rich region (left hand side). (b) The centre of a compact patch that contains fibres, which are black on account of electron scattering. The inset SAED pattern shows that the patch is nanocrystalline. (c) An organic nanoglobule within an irregular pore.

reveal the nature of materials that were accreted to form its C-complex parent body but have been lost from most other CMs. Some of the meteorite's original constituents and products of aqueous alteration have also been modified by parent body heating and terrestrial weathering. The nature of changes to the original constituents of EET 96029 are summarised in Fig. 15 and discussed below.

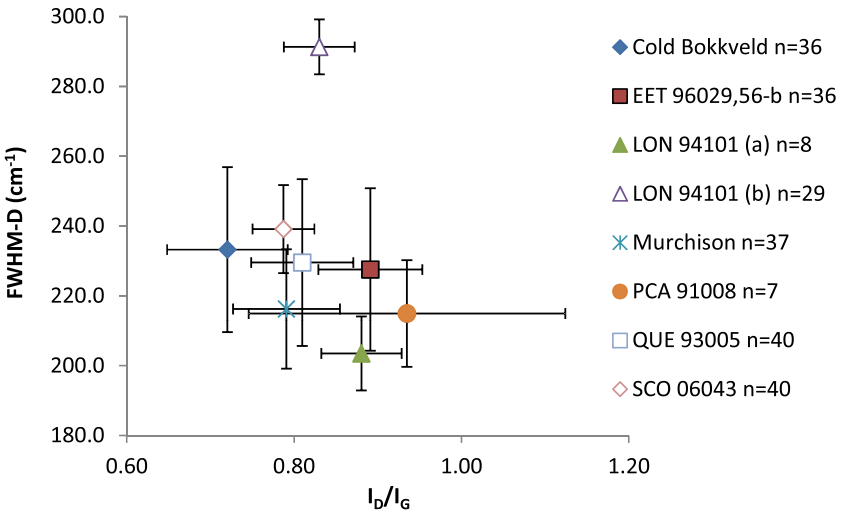

Fig. 7. Results from Raman analyses of organic matter in CM meteorites. Plotted is the full-width half maximum (FWHM) of the D band against the D/G band intensity ratio. Error bars are 1σ standard deviation.

4.1. Evaluating the degree of aqueous alteration of EET 96029

Several schemes have been proposed to quantify the degree of aqueous alteration of CM carbonaceous chondrites. Here we discuss results from EET 96029 relative to three of them with the aim of providing new insights into the nature of its parent body prior to processing by liquid water.

4.1.1. Phyllosilicate fraction

The phyllosilicate fraction metric of Howard et al. (2009, 2011, 2015) expresses the degree of aqueous alteration of CMs as the volume of phyllosilicates divided by phyllosilicates plus anhydrous silicates. A phyllosilicate fraction of <0.05 classifies the meteorite as type 3.0 (i.e., unequilibrated), and >0.95 as type 1.0 (i.e., completely altered) (Table 2). Of the 25 CMs listed in Howard et al. (2015), the least altered are both type 1.6. Assuming that the 64.7 vol.% non-crystalline component of EET 96029,57,21 was originally phyllosilicate, then this meteorite had a phyllosilicate fraction of 0.69, corresponding to type 1.6. This metric therefore indicates that EET 96029 has been very mildly altered, and so it could contain nebular materials that have been lost from most other CMs.

4.1.2. Wt.% H in water/OH

The scheme of Alexander et al. (2013) uses chemical analyses of bulk meteorite samples and is based on wt.% H (hosted by water and OH). Their alteration scale also ranges from type 3.0 (unequilibrated) to 1.0 (completely altered). The more altered CMs have higher contents of H in water/OH owing to greater abundances of phyllosilicates. After correction for H in carbonaceous material, the analysis of EET 96029 in Alexander et al. (2012) corresponds to a type 2.0, which would make EET 96029 less aqueously altered than all but one of the 54 CM meteorites listed in Alexander et al. (2013). A caveat to this conclusion is that if EET 96029 has been heated, the associated loss of water and OH could make the meteorite appear to be less aqueously altered than it was prior to thermal processing. The impact of heating on bulk H content can be estimated from the bulk δD value of EET 96029 and by making two assumptions: (i) bulk δD does not change during heating; (ii) there is a linear correlation between bulk H and δD in unheated CMs (Alexander et al., 2013). This correction suggests that before thermal processing EET 96029 may have been a type 1.4, which is again consistent with mild aqueous alteration.

4.1.3. Petrologic subtype

The discussions above suggest that prior to heating EET 96029 was phyllosilicate-poor relative to many other CMs owing to unusually mild aqueous alteration. However, these conclusions are tentative because those phyllosilicates that had formed were subsequently degraded by heating. A clearer understanding of the degree of aqueous alteration of EET 96029 may come from determining its petrologic subtype (Rubin et al., 2007) using three properties: (i) characteristics of the matrix; (ii) the nature of metal and sulphide in the matrix and chondrules; (iii) preservation of chondrule components. The scale of Rubin et al. (2007) ranges from CM3.0 (unaltered) to CM2.0 (completely altered).

4.1.3.1. Matrix characteristics. The matrices of CM2.0–2.7 meteorites are characterised by abundant phyllosilicates that have formed by aqueous alteration of nebular materials (Rubin et al., 2007; Hewins et al., 2014). The former presence of serpentine in EET 96029,9 matrix is therefore consistent with a petrologic subtype of ⩽CM2.7, although meteorites with a subtype of >CM2.7 could still contain phyllosilicates (Rubin et al., 2007). The MgO/FeO ratio of the EET 96029,9 matrix (~0.35) is low relative to that of other mildly altered CMs. For example, Rubin (2015) found that Paris matrix has a MgO/FeO ratio of 0.39,

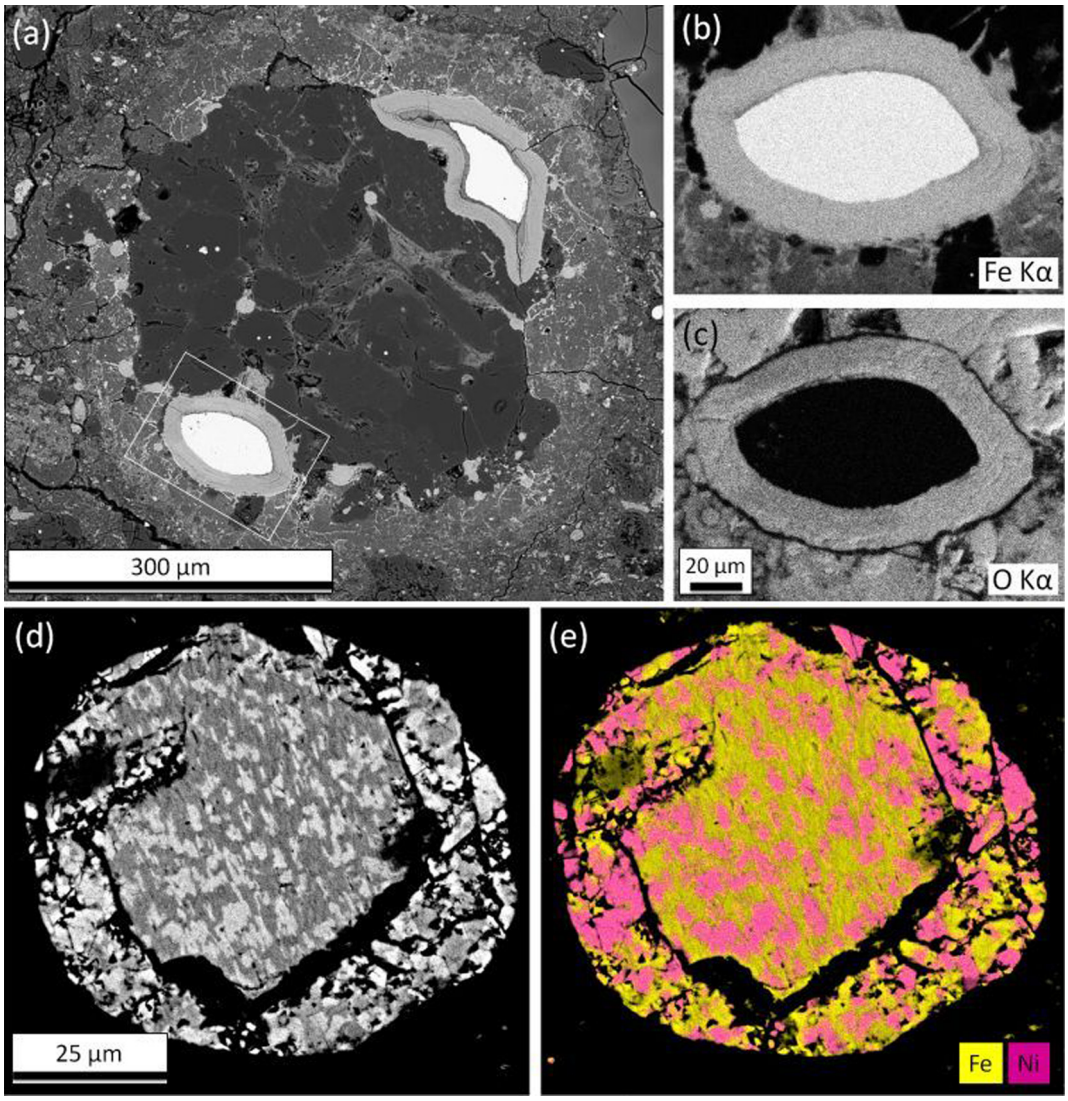

Fig. 8. Images of metal and sulphide grains in EET 96029,9. (a) BSE image of a type IAB chondrule. On the edge of the chondrule are two grains of Fe,Ni metal (white), both with concentrically layered rims. Narrow Fe-rich veins extend from these composite grains into the fine-grained rim. (b) and (c) X-ray maps of one of the grains in (a) demonstrating that its rim is rich in O and Fe. Raman spectroscopy shows that the rim is composed principally of goethite. (d) and (e) BSE image and X-ray map of a sulphide grain that contains pyrrhotite (yellow) and pentlandite (purple). (For interpretation of the references to colour in this figure legend, the reader is referred to the web version of this article.)

and combining data from two other studies gave 0.42 $\pm$ 0.02. As MgO/FeO ratios should increase in step with the degree of alteration, the low value of EET 96029,9 matrix suggests that it is more primitive than that of Paris. Sulphur concentrations also vary between meteorites, with the least altered CMs having higher values. EET 96029,9 matrix has 2.2 wt.%, in comparison to Paris with 4.2 wt.%. Whilst these differences may suggest that EET 96029,9 has been more highly altered than Paris, evidence discussed below suggests that its S was lost from EET 96029,9 matrix owing to heating of sulphides.

The fine-grained rims of EET 96029,9 contain patches of a very compact and amorphous/nanocrystalline material that may be equivalent to the amorphous material of a probable nebular origin that occurs in the matrices of the mildly altered CMs Paris and Y-791198 (Chizmadia and Brearley, 2008; Hewins et al., 2014) (Table 2). The preservation of such primitive material suggests that some parts of EET 96029 have escaped aqueous alteration, and that the meteorite has a petrologic subtype equal to or greater than Y-791198 (i.e., $\geqslant$CM2.4). The presence within EET 96029 of calcite, but absence of dolomite, indicates a petrologic subtype of $\geqslant$CM2.3 (Lee et al., 2014). The characteristics of the EET 96029 matrix therefore confirm that it has been less intensely aqueously altered than many other CMs.

4.1.3.2. Nature of metal and sulphide. Metal is a very useful indicator of the intensity of aqueous alteration of a CM carbonaceous chondrite because it is one of the most highly reactive of the primary constituents (e.g., Tomeoka and

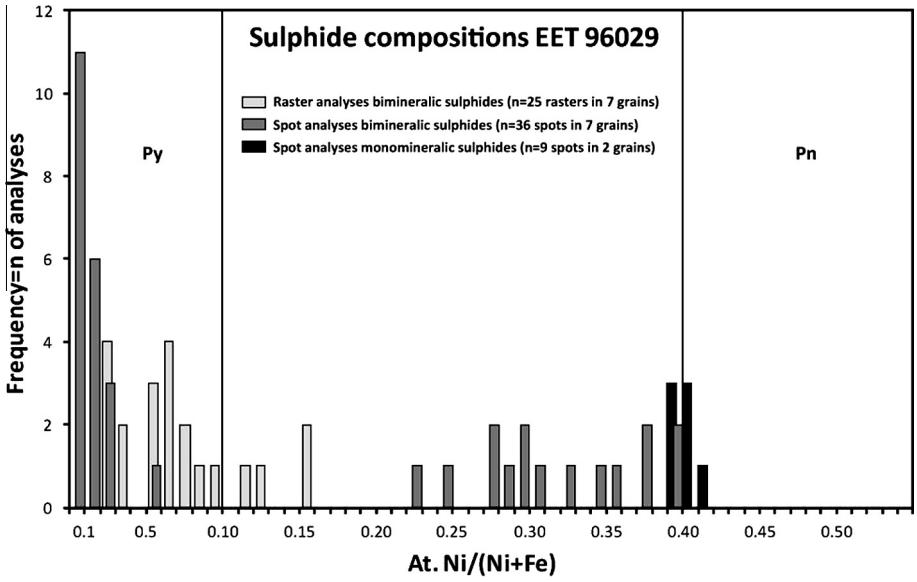

Fig. 9. Compositional range of Fe–Ni sulphides in EET 96029,9. The EDX data are plotted as atomic Ni/(Ni + Fe) ratios after Chokai et al. (2004). The fields of pyrrhotite (Py) and pentlandite (Pn) correspond to atomic Ni/(Ni + Fe) values of 0–0.10 and 0.40–0.55, respectively. Light-grey columns show raster analyses of sulphide grains containing a mixture of Ni-rich and Ni-poor areas. Medium-grey columns show spot analyses of the Ni-rich and Ni-poor areas. Dark-grey columns show spot analyses of homogeneous sulphides.

Buseck, 1985). EET 96029,9 contains 0.33 vol.% Fe,Ni metal, but also has 1.4 vol.% of Fe-(oxy)hydroxide, which is interpreted to have formed by Antarctic weathering of the metal. Thus, prior to its fall to Earth, EET 96029,9 contained as much as 1.73 vol.% Fe,Ni metal. By comparison, Paris (CM2.7) has 1.2 vol.% Fe,Ni metal (Rubin, 2014). Hence, a metal abundance of 1.73 vol.% would suggest that the aqueous alteration of EET 96029,9 has been very mild, and equivalent to a petrologic subtype of $\geqslant$CM2.7. Although metal can also be formed by heating of carbonaceous chondrites, the chemical composition and microtexture of EET 96029,9 metal is inconsistent with such an origin.

As regards to sulphides, Rubin et al. (2007) found that intermediate sulphides (atomic Ni/(Fe + Ni) ratios = 0.10–0.40), occur only in CM2.0–2.4 meteorites. Pyrrhotite and pentlandite characterise meteorites of subtypes CM2.5–2.7 (Rubin et al., 2007; Rubin, 2015). The presence of intermediate sulphides in EET96029 would therefore be consistent with a CM2.0–2.4 subtype. However, we are cautious about drawing firm conclusions from these results because many of the EET 96029,9 grains have fine-scale intergrowths of pyrrhotite with pentlandite, which indicate that these sulphides have recrystallized during heating (Kimura et al., 2011).

4.1.3.3. Preservation of chondrule components. The olivine phenocrysts and glass mesostasis of chondrules in carbonaceous chondrites are highly susceptible to aqueous alteration (e.g., Richardson, 1981). Olivine is typically replaced by veins of serpentine (Velbel et al., 2012), and such veins have been reported in meteorites of subtypes up to and including CM2.5 (Rubin et al., 2007; Lee and Lindgren, 2016). Thus, the presence of phyllosilicate veins in EET 96029 chondrule phenocrysts does not necessarily indicate a high degree of aqueous alteration.

The mesostasis of almost all chondrules in meteorites of subtypes CM2.0–2.7 contains phyllosilicates that have formed by the aqueous alteration of original glass (Rubin et al., 2007; Hewins et al., 2014). Given that chondrule EETC-4 contains glass, EET 96029 could be the first meteorite with a petrologic subtype of >CM2.7. However, EETC-4 is not unique because glass-bearing chondrules have been described from five other CMs: Murchison, Murray, Niger (I), Paris, Y-790123, and Y-75293 (Fuchs et al., 1973; Olsen and Grossman, 1978; Desnoyers, 1980; Ikeda, 1983; Metzler et al., 1992; Rubin, 2015). The compositions of some of these glasses are in Table 7 and Fig. 5a. Of these six CMs, the degree of alteration of Murchison, Murray and Paris has been studied, and all are mildly processed (Table 2). Therefore, the presence of one chondrule containing mesostasis glass is not in itself sufficient evidence to classify EET 96029 as >CM2.7, but nonetheless shows that it has been mildly altered, and at least to an equivalent level as Murchison, Murray and Paris. Glass in all of the other EET 96029,9 chondrules has been altered to phyllosilicate, and in 50% of these chondrules the mesostasis also contains quench crystallites or moulds of them. As quench crystallites also occur in the phyllosilicate mesostasis of chondrules in QUE 97990 (CM2.6; Maeda et al., 2009), their preservation may be another reliable indicator of mild aqueous alteration (i.e., a subtype of $\geqslant$CM2.6).

Glass and quench crystallites are likely to have been preserved in EET 96029,9 owing to the low porosity and permeability of the matrix and fine-grained rims (Bland et al., 2009). Porosity and permeability were probably also inhomogeneous on the sub-millimetre scale so that during early stages of aqueous alteration some chondrules were

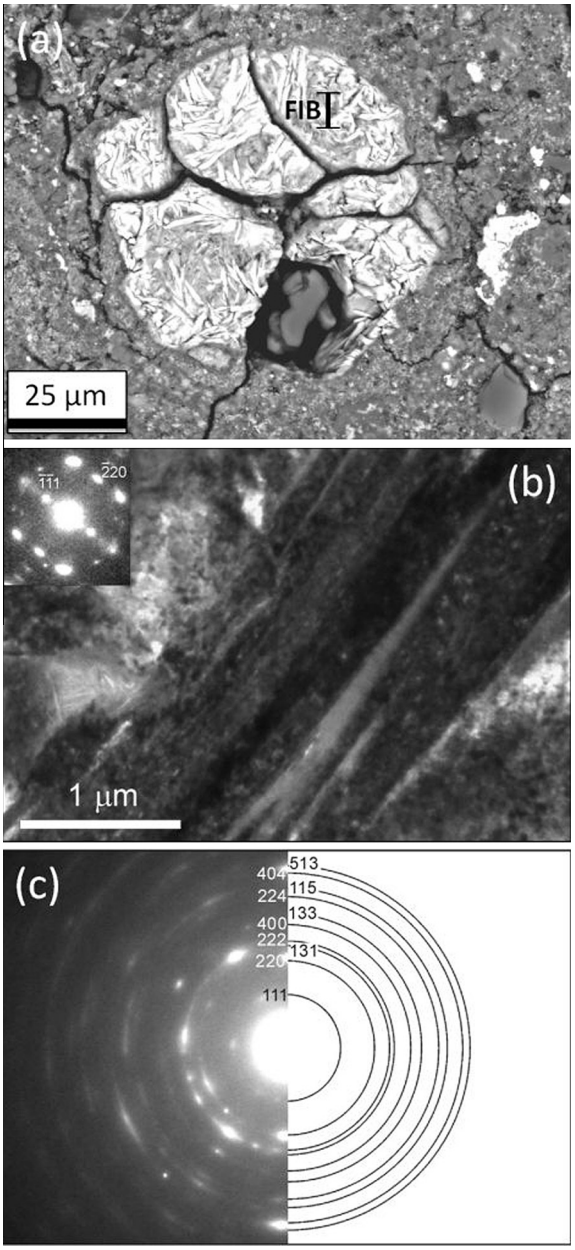

Fig. 10. A Fe–S–O clump in EET 96029,9. (a) BSE image of the clump, which has a calcite grain (grey) in its lower part. The clump contains high-Z lath-shaped grains (white) in a lower Z groundmass. (b) Bright-field TEM image of part of a foil that was extracted from the clump in (a). The midplane of this foil is delineated by "FIB". The inset SAED pattern was acquired from the centre of the lath, using a 1 μm diameter selected area aperture, and indexes as magnetite. (c) On the left hand side is part of a SAED pattern acquired from the whole lath in (b) using a 5 μm diameter selected area aperture. The right hand side shows the spacings of reflections for polycrystalline magnetite. The good correspondence between the SAED pattern and the simulation shows that the lath contains many small crystals of magnetite.

exposed to much less water than others. Within these objects the components that are most susceptible to aqueous alteration (i.e., glass) have been preserved.

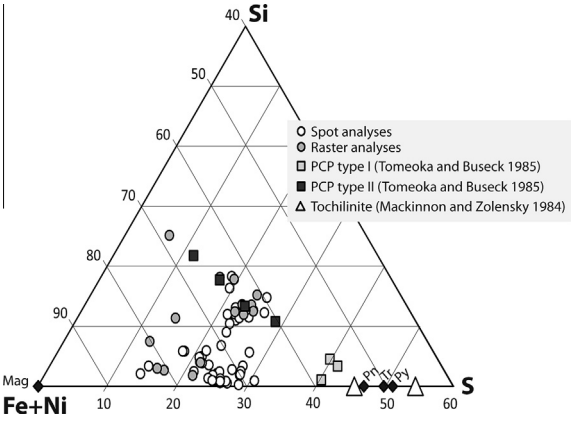

Fig. 11. Section of a ternary diagram (at.%) showing compositions of Fe–S–O clumps in EET 96029,9. Analyses were obtained in spot and raster mode (indicated by open and filled circles, respectively). Also plotted are analyses of 'PCP' and tochilinite. Ideal compositions of magnetite (Mg), pentlandite (Pn), pyrrhotite (Py) and troilite (Tr) are included for reference.

4.1.4. Mineralogy and abundance of CAIs

Rubin (2007) predicted that CAIs should be abundant in the most primitive CMs, and that some of these inclusions should also contain gehlenite. The 1.8 vol.% of CAIs in EET 96029,9 is equal to their abundance in QUE 97990 (Rubin, 2007), and considerably greater than in Paris (0.76 vol.%; Rubin, 2015), and Mighei and Cold Bokkeveld (~0.6–0.3 and ~0.01 vol.%, respectively; Rubin, 2007). The abundance of CAIs is therefore consistent with a low degree of aqueous alteration for EET 96029,9. Gehlenite is highly susceptible to aqueous alteration (Nomura and Miyamoto, 1998), and is correspondingly rare in the CMs (Greenwood et al., 1994; Lee and Greenwood, 1994; Rubin, 2007). This mineral has been described from Murchison (Armstrong et al., 1982; MacPherson et al., 1983; Simon et al., 2006) and Paris (Hewins et al., 2014; Marrocchi et al., 2014). The occurrence of gehlenite in EET 96029,9 therefore suggests that this sample of the meteorite has undergone an equivalent degree of alteration to the other two CMs (i.e., CM2.5–2.7) (Fig. 16).

4.1.5. Evidence for mild aqueous alteration of EET 96029

The properties of EET 96029 have been compared to three schemes for describing the degree of aqueous alteration of CMs, and results of these comparisons confirm that the meteorite has been very mildly processed. A caveat to this conclusion is that understanding the degree of aqueous alteration of EET 96029 is complicated by the effects of post-alteration heating and terrestrial weathering (Fig. 15). Those properties that should have been least affected by these two processes are the abundance of Fe,Ni metal, gehlenite-bearing CAIs, mesostasis glass, and mesostasis quench crystallites. Together, these properties indicate that EET 96029 has a petrologic subtype of CM2.7 and so is one of the least aqueously altered CMs yet described (Fig. 16).

Contrasts between CMs in their degree of aqueous alteration may be due to heterogeneities in the volume of water that was available. EET 96029 could have been sourced from a parent body region that had accreted relatively little water

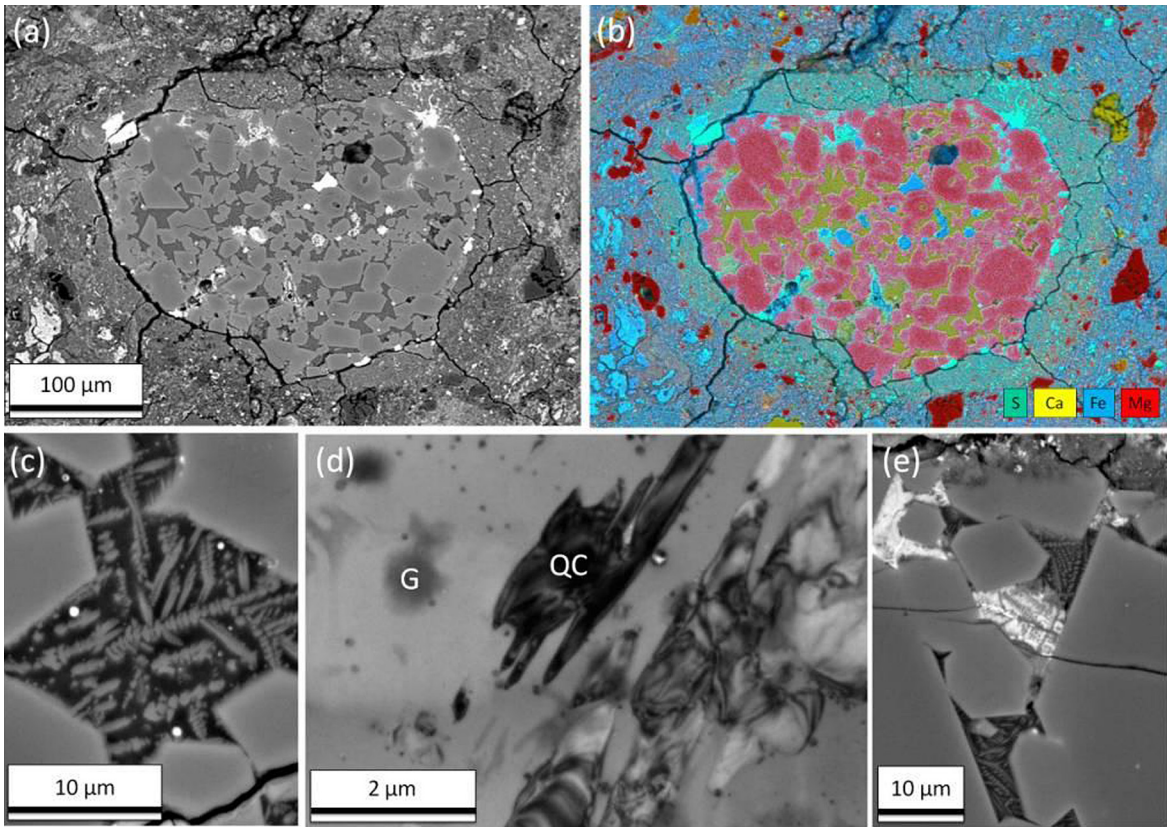

Fig. 12. Images of type IIA chondrule EETC-4 in EET 96029,9. (a) BSE image. (b) Image of the same field of view as (a) that was made by blending X-ray maps for Mg (red), S (light green), Ca (yellow) and Fe (light blue). This colouring renders the chondrule olivine pink and glass-rich mesostasis yellow-green. (c) BSE image of the unaltered chondrule interior. Euhedral olivine phenocrysts (mid-grey) enclose a Si-rich mesostasis that comprises glass (black), quench crystallites (mid-grey) and spherules of Fe-sulphide (white). (d) Bright-field TEM image of a foil cut from the Si-rich mesostasis that contains quench crystallites (QC), glass (G) and Fe-sulphide spherules (black specks). (e) BSE image of the chondrule interior with both Si- and Fe-rich mesostasis. The Fe-rich mesostasis hosts ferrihydrite (white) that encloses quench crystallites (mid-grey). (For interpretation of the references to colour in this figure legend, the reader is referred to the web version of this article.)

ice, or that had lost liquid water early, for example by fluid flow. Regarding the second possibility, the flow of water within meteorite parent bodies has been predicted by numerical simulations of their early evolution (Young et al., 2003; Travis and Schubert, 2005; Palguta et al., 2010). Until recently there has been little evidence from the meteorite record to support these models; work on the most primitive carbonaceous chondrites had suggested that the intergranular permeability was so low that fluid flow could not have taken place under the necessary timescales (Bland et al., 2009). This constraint does not however negate fluid flow via fractures, and good evidence for the movement of aqueous solutions along such high permeability conduits has been described by Lee et al. (2013). The very mild aqueous alteration of EET 96029 therefore confirms the heterogeneous availability of liquid water within the CM parent body(ies).

4.2. Heating of EET 96029

Here we explore the effects of thermal processing on the primary and secondary constituents of a mildly aqueously altered CM (Fig. 15), constrain the temperatures attained, and speculate on the heating mechanisms.

4.2.1. Dehydroxylation and amorphisation of phyllosilicates

Phyllosilicates are a sensitive indicator of the intensity of heating of an aqueously altered meteorite through the loss of water and hydroxyls, and concomitant degradation of their crystal structure. Totals obtained from the EET 96029,9 fine-grained matrix and phyllosilicate-rich chondrule mesostasis (~83.6 wt.% and ~87.8 wt.%, respectively) are high relative to analyses of the same components of CMs with no evidence for thermal processing (Fig. 4). Whilst recognising that analytical totals from X-ray microanalysis can reflect many properties other than just the content of water/OH, these findings are consistent with partial dehydroxylation upon heating. Temperatures can be constrained with reference to previous studies. For example, the loss of OH from phyllosilicates in Murchison fine-grained rims was experimentally quantified by Nakato et al. (2008). They found that pre-heating analytical totals of 80.7 wt.% increased to 87.4 wt.% after 1 h at 600 °C, and reached 93.1 wt.% after 96 h. Nakamura (2006) recorded mean totals of 92 wt.% from the matrix of Y-793321, which was inferred to have been briefly heated naturally to ~500 °C. By analogy with these experimental studies, EET 96029,9 was likely heated to <~500–600 °C.

Table 7
Chemical compositions of the Si-rich and Fe-rich mesostasis of EETC-4, and pristine mesostasis of chondrules in other CMs.

	EETC-4 mesostasis[a]		Mesostasis of other CMs	
	Si-rich	Fe-rich	Murchison[b]	Y-790123[c]
Na_2O	2.84 (1.24)	0.45 (0.22)	1.00	7.62
MgO	2.39 (0.51)	4.07 (3.29)	3.20	0.64
Al_2O_3	13.87 (0.42)	4.53 (2.95)	15.70	13.85
SiO_2	55.47 (1.81)	13.04 (8.64)	69.10	59.40
P_2O_5	0.16 (0.11)	0.20 (0.26)	–	–
S	0.13 (0.03)	1.78 (1.25)	–	–
K_2O	0.23 (0.03)	0.21 (0.58)	0.03	0.74
CaO	10.87 (0.44)	3.47 (2.74)	9.80	8.33
TiO_2	0.65 (0.03)	0.18 (0.23)	0.10	0.70
Cr_2O_3	0.13 (0.18)	0.24 (0.77)	0.10	–
MnO	0.02 (0.07)	0.04 (0.10)		0.00
FeO	10.19 (0.82)	58.13 (15.41)	0.60	8.53
Ni	d.l.	1.17 (0.43)	–	–
Total	96.94 (1.31)	87.52 (4.38)	99.63	99.79

– Denotes not analysed for.
d.l. denotes below detection limits.
[a] The present study, mean of 14 analyses for Fe-rich mesostasis and mean of 13 analyses for Si-rich mesostasis. Values in parentheses are 1σ standard deviations.
[b] Olsen and Grossman (1978), mean of eight analyses.
[c] Ikeda (1983), mean of two analyses.

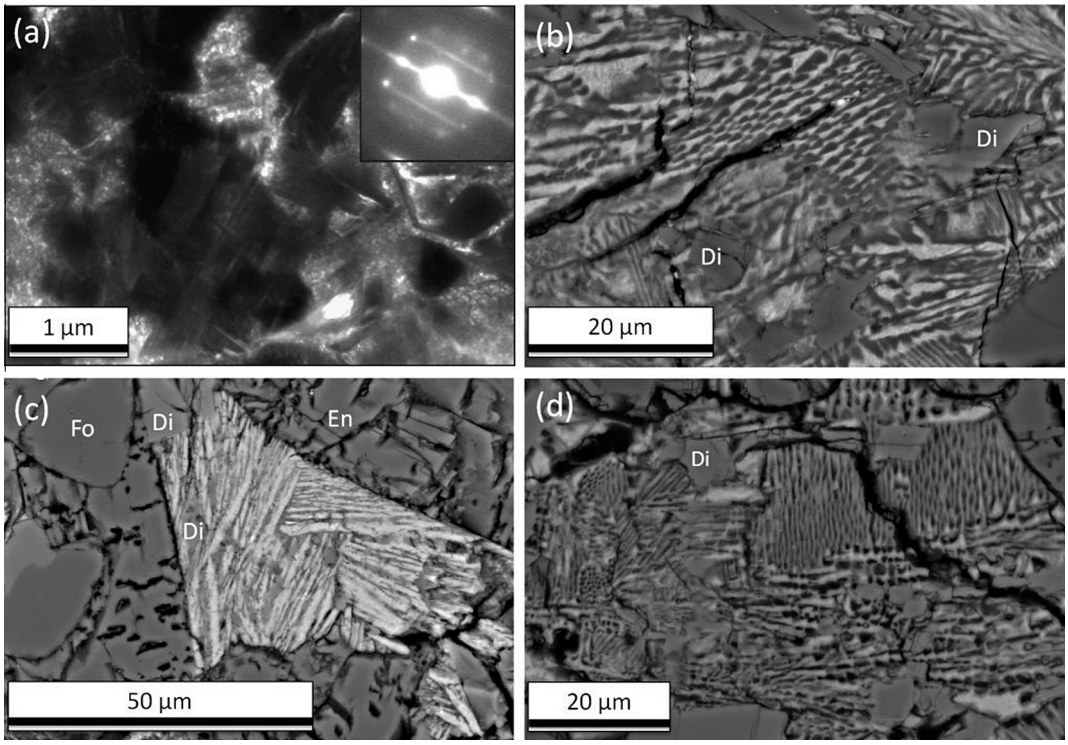

Fig. 13. Images of the mesostasis of chondrules in EET 96029,9. The minerals labelled are diopside (Di), clinoenstatite (En) and forsterite (Fo). (a) Bright-field TEM image of the mesostasis of a type II chondrule, which comprises relatively coarse grains in a finer groundmass. The inset SAED pattern is from the coarse grain in the lower left of the image, and consistent with poorly crystalline phyllosilicate. (b) and (c) BSE images of the altered mesostasis of type I chondrules, which contains quench crystallites (grey) and Fe-rich phyllosilicate (white). (d) BSE image of the altered mesostasis of a type I chondrule. Phyllosilicate (white) encloses micropores after quench crystallites (black).

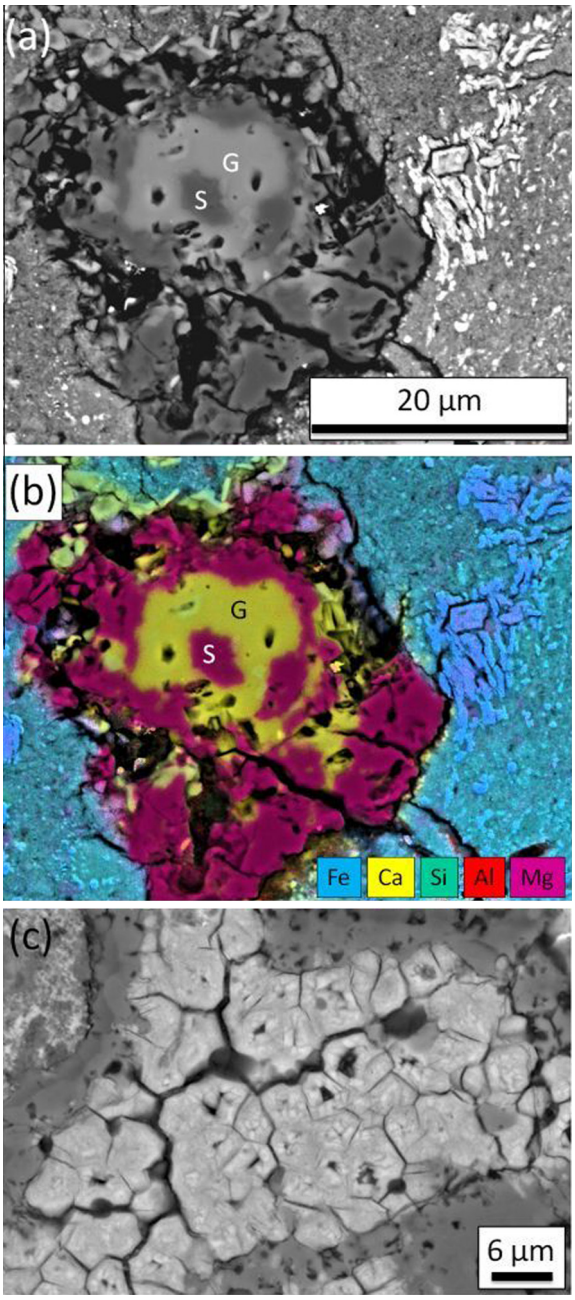

Fig. 14. (a) BSE image of a gehlenite (G) bearing CAI in EET 96029,9 that also contains spinel (S). (b) False coloured X-ray map of (a) showing the distribution of Fe (light blue), Ca (yellow), Si (light green), Al (red) and Mg (purple). (c) Phyllosilicate with a hexagonal pattern of fractures in a CAI from EET 96029-a. (For interpretation of the references to colour in this figure legend, the reader is referred to the web version of this article.)

Evidence for loss of water/OH from EET 96029 is also provided by the TGA results in Garenne et al. (2014). Their sample lost 4.5 wt.% in the 400–770 °C step, which mainly represents the dehydroxylation of phyllosilicates. This value is considerably lower than the mass loss recorded over the same temperature range for meteorites with no natural heating and a similar degree of aqueous alteration (Garenne et al., 2014). TGA results from two sub-samples of EET 96029,56,21 showed a much a greater mass loss in the 400–770 °C step (mean of 8.7 wt.%, Table 3) than was recorded by Garenne et al. (2014). There are two possible explanations for these contrasting results: (i) differences between laboratories in equipment or methodology; (ii) the NHM samples had a higher degree of aqueous alteration and/or a lower intensity of heating. In order to test the first possibility five samples of Murchison were analysed at the NHM, and in Table 3 these TGA results are compared with data from Murchison in Garenne et al. (2014). The two datasets are broadly similar and so inter-laboratory differences are unlikely to explain the contrasts between EET 96029 samples in weight loss over the 400–770 °C range. With regards to point (ii), the same sample that was used for TGA at the NHM was also studied by PSD-XRD, and results show that it has been both mildly aqueously altered and heated. The TGA data thus show that samples of EET 96029 differ in their degree of parent body processing, probably heating, owing to the presence of clasts of different lithologies.

Petrographic evidence for dehydroxylation upon heating includes the hexagonal fracture pattern within phyllosilicates from a banded CAI, and amorphisation of phyllosilicates in the chondrule mesostasis. Estimates of the temperature at which the crystal structure of serpentine breaks down range from ~400 °C (Tonui et al., 2014) to 600 °C (Nakato et al., 2008). Calcite grains show no evidence for degradation owing to heating (which for example may be recognised by formation of vesicles owing to CO_2 loss; Nakamura, 2006). Thus the matrix of EET 96029,9 did not reach the temperature at which calcite decomposes (~890 °C, Nakato et al., 2008).

4.2.2. Recrystallization of sulphides

The mineralogy and microstructure of sulphides can be used to constrain heating temperatures. Tochilinite is particularly sensitive, and estimates of its breakdown temperature range from 245 °C (Fuchs et al., 1973) to ~300 °C (Tonui et al., 2014) and ⩽600 °C (Nakato et al., 2008). The Fe–S–O clumps in the EET 96029 matrix resemble objects composed of intergrown serpentine and tochilinite that are commonplace in unheated CMs (e.g., Lee et al., 2014). However, tochilinite is absent from Fe–S–O clumps. Instead, they comprise lath-shaped aggregates of nanoscale magnetite crystals between which are poorly crystalline/amorphous grains of Mg–Fe silicate. Thus, the Fe–S–O clumps are interpreted to have formed by heating of serpentine-tochilinite aggregates; serpentine was amorphised to leave the Mg–Fe silicate grains, whereas tochilinite recrystallized to magnetite. Tomioka et al. (2007) described objects in experimentally shock-heated samples of Murchison that are petrographically and chemically very similar to the Fe–S–O clumps, and Tonui et al. (2014) confirmed that tochilinite breaks down to magnetite during artificial heating. The matrix of EET 96029,9 is depleted in S relative to Paris (Table 6), which is consistent with mobility of S during heating.

The properties of coarsely crystalline sulphide grains in the matrix are also consistent with thermal modification

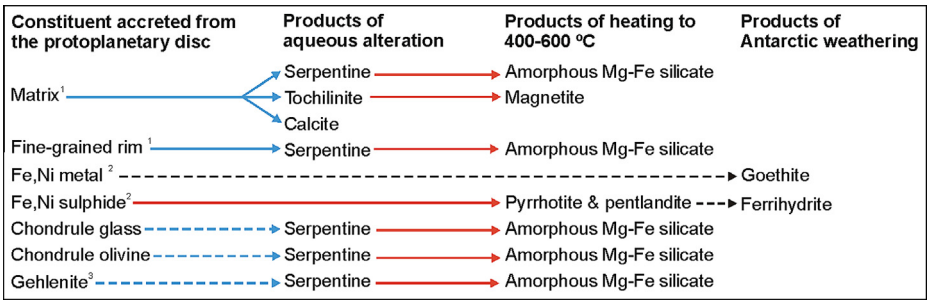

Fig. 15. Summary of changes to the original constituents of EET 96029 in response to aqueous alteration, heating, and terrestrial weathering. Solid lines indicate complete transformation of the component whereas dashed lines denote a partial transformation. Blue lines denote aqueous alteration, red lines heating, and black lines terrestrial weathering. [1]The matrix and fine-grained rims originally contained finely crystalline anhydrous silicates, metals, sulphides, and amorphous silicates. [2]Occurs in the matrix, chondrules and fine-grained rims. [3]Occurs in CAIs. Other constituents of CAIs are not included in the diagram as they have remained unchanged (i.e., spinel, hibonite, perovskite, diopside, corundum), and chondrule pyroxene is also unaltered. (For interpretation of the references to colour in this figure legend, the reader is referred to the web version of this article.)

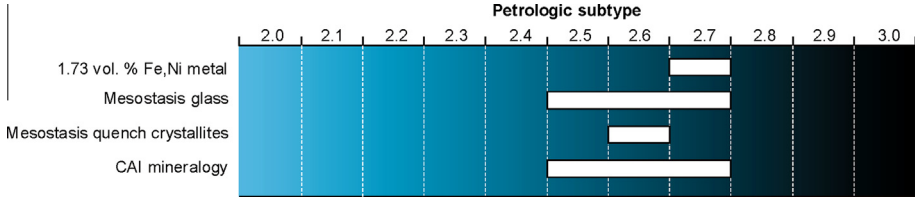

Fig. 16. The petrologic subtype of EET 96029,9. Only those properties that were most resistant to modification by heating are shown.

(Kimura et al., 2011). Seven of the nine sulphides in EET 96029,9 that were analysed quantitatively are composed of pyrrhotite with μm-sized lamellae or blebs of pentlandite, and this microtexture is consistent with temperatures of 300–750 °C (i.e., Category B of Kimura et al., 2011).

4.2.3. Structural modification of organic matter

Raman analysis of organic carbon has been used successfully to reconstruct the thermal history of terrestrial rocks (Wopenka and Pasteris, 1993; Beyssac et al., 2002; Lahfid et al., 2010) and extraterrestrial samples (Busemann et al., 2007; Beck et al., 2014; Quirico et al., 2014). This work assumes that the ordering of organic carbon increases with temperature (Beyssac et al., 2002). CM chondrites contain highly disordered carbon derived from both soluble and insoluble organic matter, and these components could have had different origins and thermal histories (Remusat et al., 2005; Quirico et al., 2014). In the present study powered samples were analysed without any prior extraction and so the Raman spectra reveal the structure of carbon in both soluble and insoluble organic matter.

Results reveal highly disordered carbon with broad D and G bands overlaying a fluorescing background. Three of the other six CMs that were studied for comparison have been heated: EET 96029, PCA 91008, QUE 93005 (Quirico et al., 2014, 2015). Results from the present study show that PCA 91008 has been most highly heated, with a high I_D/I_G and a low FWHM (D) (Fig. 7). The stronger intensity of the D band (D1) relative to the G band (D2 + G) has also been recorded in low-grade metamorphic rocks from the Swiss Alps (Lahfid et al., 2010). Here increased thermal alteration led to higher I_D/I_G and lower FWHM (D) values, in line with results of the present study. EET 96029,56-b has the second highest I_D/I_G value, thus indicating that it has been heated more than the other five CMs (Fig. 7). Although these data are consistent with heating of EET 96029,56-b, they cannot be used to constrain the timing of thermal processing relative to aqueous alteration.

The data in Fig. 7 shows that the two sub-samples of LON 94101 plot in different parts of the diagram. One sub-sample has a relatively high I_D/I_G and low FWHM (D) (more heated) and the other, with a much higher FWHM (D), plots away from the main group of samples. This range is consistent with the abundance and petrological diversity of clasts within LON 94101 (Lindgren et al., 2013) and underscores the point that clasts in CMs can have very different thermal histories.

4.2.4. Maximum temperature attained during heating

Various petrographic and mineralogical indicators enable the maximum temperature experienced by EET 96029 to be constrained. The partial dehydroxylation and amorphisation of serpentine suggests heating to >~400 °C, whereas the preservation of calcite shows that it did not reach ~890 °C. Tonui et al. (2014) suggested that chondrules begin to integrate with the matrix so that their edges become blurred if temperatures exceed 600 °C, but no such textures have been observed in the present study. These petrographic and mineralogical constraints suggest that EET 96029 was heated to between 400 and 600 °C, and probably at the lower end of that range (i.e., <500 °C). Nakamura (2005) divided heated carbonaceous chondrites into four stages (I to IV). Results from EET 96029 are consistent with Stage II, where serpentine and tochilinite

have been amorphised. Stage II corresponds to a brief period of heating to temperatures of 300–500 °C, or a longer period of heating to ~200–400 °C. Tonui et al. (2014) proposed that this four stage notation should be qualified using a prefix to describe the classification of the meteorite. Therefore EET 96029 would be a CM2TII (where "T" denotes thermal metamorphism), or if the petrologic subtype were included, a CM2.7TII.

4.3. The environment and drivers of heating

Despite the considerable literature on the effects of heating on CM carbonaceous chondrites (e.g., Nakamura, 2005; Tonui et al., 2014), the drivers of this process are poorly understood. The most common suggestion is that a brief episode of heating accompanied shock, and some CMs have evidence for a commensurately short timescale of thermal processing (Nakato et al., 2008; Yabuta et al., 2010; Orthous-Daunay et al., 2013). Shock heating is also consistent with evidence for impact deformation of some of the affected CMs; for example, Y-793321 has evidence for heating, ductile deformation and brecciation (Nakamura, 2006). As Y-793321 contains high concentrations of solar wind derived ^{4}He, ^{20}Ne and ^{36}Ar, Nakamura (2006) concluded that the meteorite had spent a considerable period of time exposed to the impactors in a parent body regolith. The heated CM MET 01072 has also undergone impact deformation, as demonstrated by the presence of flattened chondrules and a strong petrofabric (Lindgren et al., 2015).

The lack of evidence for shock deformation of other heated CMs, including PCA 91008 (Tonui et al., 2014) and EET 96029 (the present study) may be explained by the heterogeneous passage of shock waves through parent body regoliths. The alternative is to appeal to other heat sources, namely the decay of ^{26}Al or solar radiation. The former possibility is inconsistent with a short duration of thermal processing identified in other heated CMs. Radiative heating is capable of producing temperatures of >550 K over periods of hours to days in those carbonaceous asteroids with perihelia of <0.15 AU (Chaumard et al., 2012). The fact that EET 96029 is a breccia containing lithologies with contrasting hydroxyl contents would be consistent with heterogeneous heating during impacts, or with impact-mixing of parts of the regolith that had been exposed to different intensities of radiative heating. The present study provides insufficient information to discriminate between these two possibilities.

4.4. Tracking aqueous alteration and heating using oxygen isotopes

EET 96029 has good evidence for having been mildly aqueously altered and subsequently heated to ~400–600 °C. As both processes will leave their imprint on the bulk oxygen isotope composition of a carbonaceous chondrite, EET 96029 provides a good opportunity to examine and constrain their relative roles in the evolution of the oxygen isotope system.

The three EET 96029 samples analysed span almost the entire range in oxygen isotopic compositions of the CM carbonaceous chondrites. Two of the samples lie at the isotopically light end, and within the CO–CV field (Fig. 2). Hewins et al. (2014) showed that a line regressed through δ^{18}O and δ^{17}O values of multiple sub-samples of Paris passes through other CM2 falls and the CO3 falls, thus suggesting a genetic link between the two carbonaceous chondrite groups. They also noted that analyses of Paris lie close to the CO3s, thus implying that it is quite pristine. The oxygen isotope composition of EET 96029 in Tyra et al. (2007) is very similar to that of the least altered lithology of Paris. It falls precisely on the regression line through the Paris dataset, and even closer to the CO3 falls. Therefore by using the same reasoning as Hewins et al. (2014), at least one part of EET 96029 is more primitive than Paris.

One explanation for the wide range in oxygen isotope compositions of the three EET 96029 samples is intra-meteorite heterogeneity in their degree of alteration. The isotopically heavy values of EET 96029,56-c could reflect a greater degree of aqueous alteration, although the petrographic properties of the sample do not support this explanation. An alternative explanation is that EET 96029,56-c had experienced a greater intensity of heating than the other two samples. Dehydroxylation of its phyllosilicates would have been accompanied by mass-dependent isotope fractionation and loss of isotopically light water. Mayeda and Clayton (1998) showed that experimental heating of Murchison to temperatures of up to 700 °C increases its δ^{17}O and δ^{18}O values, with a maximum change in δ^{18}O of ~4‰. The 8‰ range in δ^{18}O values between samples of EET 96029 therefore suggests heating to a higher temperature and/or for a greater duration. We conclude that differences in isotopic compositions between the three samples of EET 96029 primarily reflect contrasts in temperatures and/or timescales of heating. Therefore the sample of EET 96029 that was analysed by Tyra et al. (2007) was pristine (i.e., with a low degree of aqueous alteration and low intensity of heating).

4.5. Pairing of EET 96029 and inter-meteorite heterogeneity

If EET 96029 is paired with the EET 96005 group (Grossman, 1998), then these other meteorites may help to provide a broader picture of the nature of their parent meteoroid. This pairing was questioned by Tyra et al. (2007) because EET 96029 differs to some of the other finds in its carbonate abundance and bulk oxygen isotope composition (Table 8). The oxygen isotope compositions of the two samples analysed for the present study show that EET 96029 is highly heterogeneous (Fig. 2), and this range is greater than the difference in oxygen isotope compositions between the four finds analysed by Tyra et al. (2007). Thus, oxygen isotope data cannot be used as evidence that EET 96029 is a different fall to the other ten meteorites, and we agree with Grossman (1998) that it is likely to be a member of the EET 96005 group.

If all of the finds listed in Table 8 are from the same meteoroid, their differences in oxygen isotope compositions underscore its internal heterogeneity. Analyses of EET 96006 and EET 96016 in Alexander et al. (2012) show that these two meteorites had not been heated after aqueous alteration. Thus, the meteoroid that delivered the EET

Table 8
Properties of the paired EET 96005 meteorites.

EET…	Mass (g)[a]	Weathering grade[a]	Bulk O isotope composition			Bulk H (wt.%)[d]	Bulk δD (‰)[d]	CO_2 yield (μg/g)[b]
			$\delta^{17}O$ (‰)	$\delta^{18}O$ (‰)	$\Delta^{17}O$ (‰)			
96005	1.3	B	–	–	–	–	–	–
96006	42.2	Be	0.4[b]	5.2[b]	−2.35[b]	1.276	−90.1	1470
96007	5.1	Be	–	–	–	–	–	–
96011	5.3	A	–	–	–	–	–	–
96012	9.4	Be	–	–	–	–	–	–
96013	2.1	Be	–	–	–	–	–	–
96014	2.3	B	–	–	–	–	–	–
96016	132.1	Be	2.3[b]	8.3[b]	−2.01[b]	1.249	−89.5	4140
96017	19.9	Be	0.5[b]	5.8[b]	−2.51[b]	–	–	898
96019	18.9	Be	0.4[b]	5.7[b]	−2.57[b]	–	–	1130
96029	843.3	A/B	−2.6[b]	2.4[b]	−3.82[b]	0.811	−84.8	263
96029,56-c	843.3	A/B	3.29[c]	10.82[c]	−2.34[c]	–	–	–
96029,57,21 (AK-2)	843.3	A/B	−1.21[c]	3.83[c]	−3.20[c]	–	–	–

– Not determined.
[a] Grossman (1998).
[b] Tyra et al. (2007).
[c] The present study.
[d] Alexander et al. (2012).

96005 group would have contained both heated and unheated lithologies. At least some of the heated lithologies had been very mildly aqueously altered (e.g., samples analysed for the present study). EET 96029 and its pairs can therefore provide new insights into the nature of the regolith of C-complex asteroids. In this sense the EET 96005 group would be comparable to Sutters Mill, a CM carbonaceous chondrite is a regolith breccia that contains clasts with evidence for different degrees of aqueous alteration and heating (Jenniskens et al., 2012; Beck et al., 2014).

5. CONCLUSIONS

1. EET 96029 is a regolith breccia. Different samples of this CM carbonaceous chondrite have contrasting water/hydroxyl contents and bulk oxygen isotope compositions. Such intra-meteorite heterogeneity indicates that the 843 g find contains lithologies that differ in their degree of aqueous alteration and the extent to which they have lost isotopically light oxygen due to heating. Despite the lack of evidence for shock, these different lithologies are likely to have been mixed by impacts.
2. If EET 96029 is a member of the EET 96005 paired group, then it is even more apparent that the meteoroid from which all of the finds were derived contained lithologies with contrasting degrees of aqueous alteration and intensities of heating.
3. Owing to heating, the degree of aqueous alteration of EET 96029 is difficult to quantify using schemes employing water/hydroxyl contents, and phyllosilicate abundances as measured using XRD. Those properties that were most resistant to thermal modification (e.g., occurrence of Fe,Ni metal, mesostasis glass, gehlenite) indicate that EET 96029 contains very mildly aqueously altered lithologies that have a petrologic subtype of CM2.7. This conclusion is consistent with the unusually light bulk oxygen isotope compositions of two samples of EET 96029.
4. Petrographic evidence for heating of EET 96029 after aqueous alteration includes the partial dehydroxylation and amorphisation of serpentine, replacement of tochilinite by magnetite and concomitant loss of sulphur from the matrix. The maximum temperatures attained were between 400 and 600 °C, and probably at the lower end of that range. EET 96029 can be classified as CM2.7TII. It remains unknown whether the agent of heating was impacts or solar radiation.
5. EET 96029 has provided new insights into the nature and history of carbonaceous chondrite parent body regoliths, and such information will be crucial in the evaluation of results from future missions to return samples of C-complex asteroids.

ACKNOWLEDGEMENTS

We thank the NHM London and NASA ANSMET for loan of the meteorite samples. We are also grateful for technical assistance from Peter Chung, William Smith, Colin How and Sam McFadzean. Eric Quirico is thanked for discussions about Raman data processing, and we acknowledge helpful comments from Gregory Herzog, Eric K. Tonui and two anonymous reviewers. This work was funded by the UK Science and Technology Facilities Council through Grants ST/H002960/1, ST/K000942/1, ST/L002167/1 and ST/J001473/1.

APPENDIX A. SUPPLEMENTARY DATA

Supplementary data associated with this article can be found, in the online version, at http://dx.doi.org/10.1016/j.gca.2016.05.008.

REFERENCES

Abreu N. M. and Brearley A. J. (2010) Early solar system processes recorded in the matrices of two highly pristine CR3 carbonaceous chondrites, MET 00426 and QUE 99177. *Geochim. Cosmochim. Acta* **74**, 1146–1171.

Akai J. (1988) Incompletely transformed serpentine-type phyllosilicates in the matrix of Antarctic CM chondrites. *Geochim. Cosmochim. Acta* **74**, 1593–1599.

Akai J. (1990) Thermal metamorphism in four Antarctic carbonaceous chondrites and its temperature scale estimated by T-T–T diagram. In *Antarct. Meteorit. XV. Tokyo, Natl. Inst. Polar Res.*, pp. 86–87.

Alexander C. M. O'D., Bowden R., Fogel M. L., Howard K. T., Herd C. D. K. and Nittler L. R. (2012) The provenances of asteroids, and their contributions to the volatile inventories of the terrestrial planets. *Science* **337**, 721–723.

Alexander C. M. O'. D., Howard K. T., Bowden R. and Fogel M. L. (2013) The classification of CM and CR chondrites using bulk H, C and N abundances and isotopic compositions. *Geochim. Cosmochim. Acta* **123**, 244–260.

Armstrong J. T., Meeker G. P., Huneke J. C. and Wasserburg G. J. (1982) The Blue Angel: I. The mineralogy and petrogenesis of a hibonite inclusion from the Murchison meteorite. *Geochim. Cosmochim. Acta* **46**, 575–595.

Batchelder M. and Cressey G. (1998) Rapid, accurate phase quantification of clay-bearing samples using a position-sensitive X-ray detector. *Clays Clay Miner.* **46**, 183–194.

Beck P., Quirico E., Garenne A., Yin Q.-Z., Bonal L., Schmitt B., Montes-Hernandez G., Montagnac G., Chiriac R. and Toche F. (2014) The secondary history of Sutter's Mill CM carbonaceous chondrite based on water abundance and the structure of its organic matter from two clasts. *Meteorit. Planet. Sci.* **49**, 2064–2073.

Beyssac O., Goffé B., Chopin C. and Rouzaud J. N. (2002) Raman spectra of carbonaceous material in metasediments: a new geothermometer. *J. Met. Geol.* **20**, 859–871.

Bland P. A., Jackson M. D., Coker R. F., Cohen B. A., Webber J. B. W., Lee M. R., Duffy C. M., Chater R. J., Ardakani M. G., McPhail D. S., McComb D. W. and Benedix G. K. (2009) Why aqueous alteration in asteroids was isochemical: high porosity ≠ high permeability. *Earth Planet. Sci. Lett.* **287**, 559–568.

Brearley A. J. (1993) Matrix and fine-grained rims in the unequilibrated CO3 chondrite, ALHA77307 – origins and evidence for diverse, primitive nebular dust components. *Geochim. Cosmochim. Acta* **57**, 1521–1550.

Browning L. B., McSween H. Y. and Zolensky M. E. (1996) Correlated alteration effects in CM carbonaceous chondrites. *Geochim. Cosmochim. Acta* **60**, 2621–2633.

Bunch T. E. and Chang S. (1980) Carbonaceous chondrites-II. Carbonaceous chondrite phyllosilicates and light element geochemistry as indicators of parent body processes and surface conditions. *Geochim. Cosmochim. Acta* **44**, 1543–1577.

Busemann H., Alexander C. M. O'. D. and Nittler L. R. (2007) Characterization of insoluble organic matter in primitive meteorites by microRaman spectroscopy. *Meteorit. Planet. Sci.* **42**, 1387–1416.

Chaumard N., Devouard B., Delbo M., Provost A. and Zanda B. (2012) Radiative heating of carbonaceous near-Earth objects as a cause of thermal metamorphism for CK chondrites. *Icarus* **220**, 65–73.

Chizmadia L. J. and Brearley A. J. (2008) Mineralogy, aqueous alteration, and primitive textural characteristics of fine-grained rims in the Y-791198 CM2 carbonaceous chondrite: TEM observations and comparison to ALHA 81002. *Geochim. Cosmochim. Acta* **72**, 602–625.

Chokai J., Zolensky M., Le L., Nakamura K., Mikouchi T., Monkawa A., Koizumi E. and Miyamoto M. (2004) Aqueous alteration mineralogy in CM carbonaceous chondrites. *Lunar Planet. Sci. XXXV*. #1506 (abstr.).

Clayton R. N. and Mayeda T. K. (1999) Oxygen isotope studies of carbonaceous chondrites. *Geochim. Cosmochim. Acta* **63**, 2089–2104.

Cloutis E. A., Hudon P., Hiroi T., Gaffey M. J. and Mann P. (2012) Spectral reflectance properties of carbonaceous chondrites: 8. "Other" carbonaceous chondrites: CH, ungrouped, polymict, xenolithic inclusions, and R chondrites. *Icarus* **221**, 984–1001.

Desnoyers C. (1980) The Niger(I) carbonaceous chondrite and implications for the origin of aggregates and isolated olivine grains in CV2 chondrites. *Earth Planet. Sci. Lett.* **47**, 223–234.

Fuchs L. H., Olsen E. and Jensen K. J. (1973) Mineralogy, mineral chemistry, and composition of the Murchison (C2) meteorite. *Smithson. Contrib. Earth Sci.* **10**, 39.

Garenne A., Beck P., Montes-Hernandez G., Chiriac R., Toche F., Quirico E., Bonal L. and Schmitt B. (2014) The abundance and stability of "water" in type 1 and 2 carbonaceous chondrites (CI, CM and CR). *Geochim. Cosmochim. Acta* **137**, 93–112.

Greenwood R. C., Lee M. R., Hutchison R. and Barber D. J. (1994) Formation and alteration of CAIs in Cold Bokkeveld (CM2). *Geochim. Cosmochim. Acta* **58**, 1913–1935.

Greshake A. (1997) The primitive matrix components of the unique carbonaceous chondrite Acfer 094: a TEM study. *Geochim. Cosmochim. Acta* **61**, 437–452.

Grimm R. E. and McSween, Jr., H. Y. (1989) Water and the thermal evolution of carbonaceous chondrite parent bodies. *Icarus* **82**, 244–280.

Grossman J. N. (1998) The meteoritical bulletin, No. 82, 1998 July. *Meteorit. Planet. Sci. Supp.* **33**, A221–A239.

Grossman J. N. and Zipfel J. (2001) The meteoritical bulletin, No. 85, 2001 September. *Meteorit. Planet. Sci. Supp.* **36**, A293–A322.

Haack H., Grau T., Bischoff A., Horstmann M., Wasson J., Sorensen A., Laubenstein M., Ott U., Palme H., Gellissen M., Greenwood R. C., Pearson V. K., Franchi I. A., Gabelica Z. and Schmitt-Kopplin P. (2012) Maribo – a new CM fall from Denmark. *Meteorit. Planet. Sci.* **47**, 30–50.

Hanowski N. P. and Brearley A. J. (2001) Aqueous alteration of chondrules in the CM carbonaceous chondrite, Allan Hills 81002: implications for parent body alteration. *Geochim. Cosmochim. Acta* **65**, 495–518.

Hewins R. H., Bourot-Denise M., Zanda B., Leroux H., Barrat J.-A., Humayun M., Göpel C., Greenwood R. C., Franchi I. A., Pont S., Lorand J.-P., Cournède C., Gattacceca J., Rochette P., Kuga M., Marrocchi Y. and Marty B. (2014) The Paris meteorite, the least altered CM chondrite so far. *Geochim. Cosmochim. Acta* **124**, 190–222.

Howard K. T., Benedix G. K., Bland P. A. and Cressey G. (2009) Modal mineralogy of CM2 chondrites by X-ray diffraction (PSD-XRD). Part 1: total phyllosilicate abundance and the degree of aqueous alteration. *Geochim. Cosmochim. Acta* **73**, 4576–4589.

Howard K. T., Benedix G. K., Bland P. A. and Cressey G. (2011) Modal mineralogy of CM chondrites by X-ray diffraction (PSD-XRD). Part 2: degree, nature and settings of aqueous alteration. *Geochim. Cosmochim. Acta* **75**, 2735–2751.

Howard K. T., Alexander C. M. O'. D., Schrader D. L. and Dyl K. A. (2015) Classification of hydrous meteorites (CR, CM and C2 ungrouped) by phyllosilicate fraction: PSD-XRD modal mineralogy and planetesimal environments. *Geochim. Cosmochim. Acta* **149**, 206–222.

Ikeda Y. (1983) Alteration of chondrules and matrices in the four Antarctic carbonaceous chondrites ALH-77307(C3), Y-790123 (C2), Y-75293(C2), and Y-74662(C2). In *Antarct. Meteorit. VIII. Tokyo, Natl. Inst. Polar Res.*, pp. 93–108.

Janney D. E., Cowley J. M. and Buseck P. R. (2000) Transmission electron microscopy of synthetic 2- and 6-line ferrihydrite. *Clays Clay Miner.* **48**, 111–119.

Jenniskens P., Fries M. D., Yin Q.-Z., Zolensky M., Krot A. N., Sandford S. A., Sears D., Beauford R., Ebel D. S., Friedrich J. M., Nagashima K., Wimpenny J., Yamakawa A., Nishiizumi K., Hamajima Y., Caffee M. W., Welten K. C., Laubenstein M., Davis A. M., Simon S. B., Heck P. R., Young E. D., Kohl I. E., Thiemens M. H., Nunn M. H., Mikouchi T., Hagiya K., Ohsumi K., Cahill T. A., Lawton J. A., Barnes D., Steele A., Rochette P., Verosub K. L., Gattacceca J., Cooper G., Glavin D. P., Burton A. S., Dworkin J. P., Elsila J. E., Pizzarello S., Ogliore R., Schmitt-Kopplin P., Harir M., Hertkorn N., Verchovsky A., Grady M., Nagao K., Okazaki R., Takechi H., Hiroi T., Smith K., Silber E. A., Brown P. G., Albers J., Klotz D., Hankey M., Matson R., Fries J. A., Walker R. J., Puchtel I., Lee C.-T., Erdman M. E., Eppich G. R., Roeske S., Gabelica Z., Lerche M., Nuevo M., Girten B. and Worden S. P. (2012) Radar enabled recovery of the Sutter's Mill meteorite, a carbonaceous chondrite regolith breccia. *Science* **338**, 1583–1587.

Kimura M., Grossman J. N. and Weisberg M. K. (2011) Fe–Ni metal and sulphide minerals in CM chondrites: an indicator for thermal history. *Meteorit. Planet. Sci.* **46**, 431–442.

King A. J., Solomon J. R., Schofield P. F. and Russell S. S. (2015a) Characterising the CI and CI-like carbonaceous chondrites using thermogravimetric analyses and infrared spectroscopy. *Earth Planets Space* **67**, 198.

King A. J., Schofield P. F., Howard K. T. and Russell S. S. (2015b) Modal mineralogy of CI and CI-like chondrites by X-ray diffraction. *Geochim. Cosmochim. Acta* **165**, 148–160.

Lahfid A., Beyssac O., Deville E., Negro F., Chopin C. and Goffé B. (2010) Evolution of the Raman spectrum of carbonaceous material in low-grade metasediments of the Glarus Alps (Switzerland). *Terra Nova* **22**, 354–360.

Lee M. R. and Greenwood R. C. (1994) Alteration of calcium- and aluminium-rich inclusions (CAIs) in the Murray (CM2) carbonaceous chondrite. *Meteoritics* **29**, 780–790.

Lee M. R. and Lindgren P. (2016) Aqueous alteration of chondrules from the Murchison CM carbonaceous chondrite: replacement, pore filling and the genesis of polyhedral serpentine. *Meteorit. Planet. Sci.* http://dx.doi.org/10.1111/maps.12644.

Lee M. R., Bland P. A. and Graham G. (2003) Preparation of TEM samples by focused ion beam (FIB) techniques: applications to the study of clays and phyllosilicates in meteorites. *Min. Mag.* **67**, 581–592.

Lee M. R., Sofe M. R., Lindgren P., Starkey N. A. and Franchi I. A. (2013) The oxygen isotope evolution of parent body aqueous solutions as recorded by multiple carbonate generations in the Lonewolf Nunataks 94101 CM2 carbonaceous chondrite. *Geochim. Cosmochim. Acta* **121**, 452–466.

Lee M. R., Lindgren P. and Sofe M. R. (2014) Aragonite, breunnerite, calcite and dolomite in the CM carbonaceous chondrites: high fidelity recorders of progressive parent body aqueous alteration. *Geochim. Cosmochim. Acta* **144**, 126–156.

Lindgren P., Lee M. R., Sofe M. R. and Zolensky M. E. (2013) Clasts in the CM2 carbonaceous chondrite Lonewolf Nunataks 94101: evidence for aqueous alteration prior to complex mixing. *Meteorit. Planet. Sci.* **48**, 1074–1090.

Lindgren P., Hanna R. D., Dobson K. J., Tomkinson T. and Lee M. R. (2015) The paradox between low shock-stage and evidence for compaction in CM carbonaceous chondrites explained by multiple low-intensity impacts. *Geochim. Cosmochim. Acta* **148**, 159–178.

MacPherson G. J., Bar Matthews M., Tanaka T., Olsen E. and Grossman L. (1983) Refractory inclusions in the Murchison meteorite. *Geochim. Cosmochim. Acta* **47**, 823–839.

Maeda M., Tomeoka K. and Seto Y. (2009) Early aqueous alteration process in the QUE 97990 and Y791198 CM carbonaceous chondrites. *J. Min. Petrol. Sci.* **104**, 92–96.

Marrocchi Y., Gounelle M., Blanchard I., Caste F. and Kearsley A. T. (2014) The Paris meteorite: secondary minerals and asteroidal processing. *Meteorit. Planet. Sci.* **49**, 1232–1249.

Mayeda T. K. and Clayton R. N. (1998) Oxygen isotope effects in serpentine dehydration. *Lunar Planet. Sci. XXIX*. #1405 (abstr.).

McSween H. Y. (1979) Alteration in CM carbonaceous chondrites inferred from modal and chemical variations in matrix. *Geochim. Cosmochim. Acta* **43**, 1761–1770.

Metzler K., Bischoff A. and Stoffler D. (1992) Accretionary dust mantles in CM chondrites: evidence for solar nebula processes. *Geochim. Cosmochim. Acta* **56**, 2873–2897.

Miller M. F., Franchi I. F., Sexton A. S. and Pillinger C. T. (1999) High precision $\Delta^{17}O$ isotope measurements of oxygen from silicates and other oxides: methods and applications. *Rapid Commun. Mass Spectrom.* **13**, 1211–1217.

Moriarty G. M., Rumble, III, D. and Friedrich J. M. (2009) Compositions of four unusual CM or CM-related Antarctic chondrites. *Chem. Erde – Geochem.* **69**, 161–168.

Nakamura T. (2005) Post-hydration thermal metamorphism of carbonaceous chondrites. *J. Min. Petrol. Sci.* **100**, 260–272.

Nakamura T. (2006) Yamato 793321 CM chondrite: dehydrated regolith material of a hydrous asteroid. *Earth Planet. Sci. Lett.* **242**, 26–38.

Nakato A., Nakamura T., Kitajima F. and Noguchi T. (2008) Evaluation of dehydration mechanism during heating of hydrous asteroids based on mineralogical and chemical analysis of naturally and experimentally heated CM chondrites. *Earth Planets Space* **60**, 855–864.

Nomura K. and Miyamoto M. (1998) Hydrothermal experiments on alteration of Ca–Al-rich inclusions (CAIs) in carbonaceous chondrites: implication for aqueous alteration in parent asteroids. *Geochim. Cosmochim. Acta* **62**, 3575–3588.

Olsen E. and Grossman L. (1978) Origin of isolated olivine grains in type-2 carbonaceous chondrites. *Earth Planet. Sci. Lett.* **41**, 111–127.

Orthous-Daunay F. R., Quirico E., Beck P., Brissaud O., Dartois E., Pino T. and Schmitt B. (2013) Mid-infrared study of the molecular structure variability of insoluble organic matter from primitive chondrites. *Icarus* **223**, 534–543.

Palguta J., Schubert G. and Travis B. J. (2010) Fluid flow and chemical alteration in carbonaceous chondrite parent bodies. *Earth Planet. Sci. Lett.* **296**, 235–243.

Pernet-Fisher J. F., Howarth G. H., Barry P. H., Bodnar R. J. and Taylor L. A. (2014) The extent of aqueous alteration within the Jbilet Winselwan CM2 chondrite. *Lunar Planet. Sci. XLV*. #2386 (abstr.).

Quirico E., Orthous-Daunay F.-R., Beck P., Bonal L., Brunetto R., Dartois E., Pino T., Montagnac G., Rouzaud J.-N., Engrand C. and Duprat J. (2014) Origin of insoluble organic matter in type 1 and 2 chondrites: new clues, new questions. *Geochim. Cosmochim. Acta* **136**, 80–99.

Quirico E., Bonal L., Flandinet L. and Beck P. (2015) Rating thermal metamorphism in C2 chondrites with insoluable organic matter. *78th Annual Meteoritical Society Meeting*. #5090 (abstr.).

Remusat L., Derenne S., Robert F. and Knicker H. (2005) New pyrolytic and spectroscopic data on Orgueil and Murchison

Insoluble Organic Matter: a different origin than soluble? *Geochim. Cosmochim. Acta* **69**, 3919–3932.

Richardson S. M. (1981) Alteration of mesostasis in chondrules and aggregates from three C2 carbonaceous chondrites. *Earth Planet. Sci. Lett.* **52**, 67–75.

Righter K. L. (2010). *Antarct. Meteorite Newslett.* **33**(1), 4.

Rubin A. E. (2007) Petrography of refractory inclusions in CM2.6 QUE 97990 and the origin of melilite-free spinal inclusions in CM chondrites. *Meteorit. Planet. Sci.* **42**, 1711–1729.

Rubin A. E. (2014) Degree of aqueous alteration in CM2 Paris and the petrography of its refractory and amoeboid inclusions. *Lunar Planet. Sci. XLV*. #1130 (abstr.).

Rubin A. E. (2015) An American on Paris: extent of aqueous alteration of a CM chondrite and the petrography of its refractory and amoeboid olivine inclusions. *Meteorit. Planet. Sci.* **50**, 1595–1612.

Rubin A. E., Trigo-Rodriguez J. M., Huber H. and Wasson J. T. (2007) Progressive aqueous alteration of CM carbonaceous chondrites. *Geochim. Cosmochim. Acta* **71**, 2361–2382.

Simon S. B., Grossman L., Hutcheon I. D., Phinney D. L., Weber P. K. and Fallon S. J. (2006) Formation of spinel-, hibonite-rich inclusions found in CM2 carbonaceous chondrites. *Am. Min.* **91**, 1675–1687.

Tomeoka K. and Buseck P. R. (1985) Indicators of aqueous alteration in CM carbonaceous chondrites: microtextures of a layered mineral containing Fe, S, O and Ni. *Geochim. Cosmochim. Acta* **49**, 2149–2163.

Tomioka N., Tomeoka K., Nakamura-Messenger K. and Sekine T. (2007) Heating effects of the matrix of experimentally shocked Murchison CM chondrite: comparison with micrometeorites. *Meteorit. Planet. Sci.* **42**, 19–30.

Tonui E. K., Zolensky M. E., Lipschutz M. E., Wang M.-S. and Nakamura T. (2003) Yamato 86029: aqueously altered and thermally metamorphosed CI-like chondrite with unusual textures. *Meteorit. Planet. Sci.* **38**, 269–292.

Tonui E., Zolensky M., Hiroi T., Nakamura T., Lipschultz M. E., Wang M.-S. and Okudaira K. (2014) Petrographic, chemical and spectroscopic evidence for thermal metamorphism in carbonaceous chondrites I: CI and CM chondrites. *Geochim. Cosmochim. Acta* **126**, 284–306.

Travis B. J. and Schubert G. (2005) Hydrothermal convection in carbonaceous chondrite parent bodies. *Earth Planet. Sci. Lett.* **407**, 234–250.

Tyra M. A., Farquhar J., Wing B. A., Benedix G. K., Jull A. J. T., Jackson T. and Thiemens M. H. (2007) Terrestrial alteration of carbonate in a suite of Antarctic CM chondrites: evidence from oxygen and carbon isotopes. *Geochim. Cosmochim. Acta* **71**, 782–795.

Velbel M. A., Tonui E. K. and Zolensky M. E. (2012) Replacement of olivine by serpentine in the carbonaceous chondrite Nogoya (CM2). *Geochim. Cosmochim. Acta* **87**, 117–135.

Wopenka B. and Pasteris J. D. (1993) Structural characterization of kerogens to granulite-facies graphite: applicability of Raman microprobe spectroscopy. *Am. Min.* **78**, 533–557.

Yabuta H., Alexander C. M. O'. D., Fogel M. L., Kilcoyne A. L. D. and Cody G. D. (2010) A molecular and isotopic study of the macromolecular organic matter of the ungrouped C2 WIS 91600 and its relationship to Tagish Lake and PCA 91008. *Meteorit. Planet. Sci.* **45**, 1446–1460.

Young E. D., Zhang K. and Schubert G. (2003) Conditions for pore water convection within carbonaceous chondrite parent bodies: implications for planetesimal size and heat production. *Earth Planet. Sci. Lett.* **213**, 249–259.

Associate editor: Gregory F. Herzog